Prepared for submission to SPSC

Light dark matter search with positron beams at NA64

The NA64 Collaboration[1]

Abstract: We propose to extend the current NA64 scientific program to include a positron-beam, missing-energy search for light dark matter (LDM) in the mass region above 100 MeV, exploiting the high-quality CERN e^+ beam at the SPS H4 beamline. After an initial R&D phase, we plan to run a multi-stage measurement, varying the energy of the beam in order to fully exploit the resonant signature of the LDM production via e^+e^- annihilation. Specifically, we propose to run a first phase at 60 GeV beam energy, accumulating up to 10^{11} positrons-on-target, followed by a 40 GeV measurement with the same accumulated statistics. This experimental program will allow NA64 to explore the LDM parameter space in the mass range between 135 MeV and 250 MeV, probing for the first time the so-called "thermal target lines", i.e the value of the dark sector coupling predicted by astrophysical and cosmological arguments, for selected values of the model parameters, in the aforementioned mass range. Based on the obtained results, we also envisage to perform subsequent measurements to accumulate further statistics and explore further regions of the LDM parameter space.

We plan to run the experiment exploiting the existing NA64 setup, with specific upgrades necessary to match the detector performances to the lower-energy kinematic regime. Thanks to the versatility of the H4 beamline, we will be able to perform each positron measurement at the end of the main electron-beam runs, thus maximizing the efficiency of use of the H4 beam.

CERN-SPSC-2024-003 / SPSC-P-348-ADD-4
29/01/2024

[1] http://na64.web.cern.ch/

Contents

Executive summary

Thermal dark matter models with LDM particles χ with mass m_χ below the electroweak scale can provide an attractive explanation for the observed relic dark matter (DM) density. The model motivates the existence of a new feeble interaction between the dark and ordinary matter via a light mediator. The NA64 experiment at the CERN SPS was designed to probe light sub-GeV DM (LDM) production in invisible decays of a dark vector mediator, called the dark photon (A'), in collisions of 100 GeV electrons with the active target at the CERN SPS by using the missing-energy technique. Running for the last decade in electron mode, NA64 has successfully completed its primary goals and reached the world's best sensitivity in probing for the first time the well-motivated region of parameter space of benchmark thermal scalar and fermionic dark matter models with $\simeq 10^{12}$ electrons on target (EOT). The most sensitive limits on the A' couplings to photons for masses $m_{A'} \lesssim 0.35$ GeV were set excluding scalar and Majorana dark matter with the $\chi - A'$ coupling $\alpha_D \leq 0.1$ for masses 1 MeV $\lesssim m_\chi \lesssim$ 100 MeV, assuming $3m_\chi \leq m_{A'}$. However, for the mass range $m_\chi \gtrsim 100$ MeV the search is now affected by the low LDM production cross section, such that accumulating more EOT will not provide significantly improved sensitivity to probe this region. This proposal to the CERN SPSC, fully complementary to the ongoing NA64 missing-energy LDM search with a 100 GeV electron beam, presents a new opportunity for the NA64 experiment to overcome this challenge and to carry out a sensitive search for LDM in the high mass range by exploiting the resonant signature of the LDM production via e^+e^- annihilation.

Specifically, we propose to use a positron beam impinging on the NA64 active thick target to search for LDM produced via the resonant annihilation of the primary positron and its secondaries with atomic electrons. The annihilation reaction involves the exchange of an on-shell dark photon ($e^+e^- \to A' \to \chi\overline{\chi}$), acting as a mediator between the Standard Model and the Dark Sector. Thanks to the resonant nature of the process, the signal yield is strongly enhanced in the allowed kinematic region. Furthermore, this reaction is characterized by a unique signature of the signal, manifesting itself as a narrow peak in the missing energy distribution, whose position solely depends on the A' mass value. This signature will allow us to employ advanced background rejection techniques and, in case of a positive observation, to directly measure the dark photon mass.

The idea of exploiting the e^+e^- annihilation channel to enhance LDM production in the $\simeq 100$ MeV mass region has been already successfully exploited by NA64. Specifically, this signal production mechanism has been recently included in the analysis of the electron-beam data, by considering the contribution of secondary positrons in the e^--induced EM shower. The corresponding LDM yield enhancement allowed us to exclude the LDM existence down to the "thermal-target" region for $m_{A'} \simeq 250$ MeV. Furthermore, a successful low-statistics e^+ pilot run was completed in summer 2022 using the 100 GeV positron beam from the H4 beamline and the existing NA64 setup. Despite the reduced statistics, the obtained results demonstrated the feasibility of the new experimental technique, and were used as a solid guidance to design the proposed measurement [1].

These efforts demonstrated the unique potential of a positron-beam missing energy

search for LDM at CERN. The experimental program proposed in this document consists in a multi-stage positron-beam measurement, varying the primary beam energy to scan the A' mass range via the resonant technique. We point out that the exceptional properties of the CERN H4 positron beam in terms of beam quality, capability of energy tuning, and reduced contamination provide a unique opportunity to either discover or rule out thermal LDM in the $m_{A'} \gtrsim 100$ MeV region in the near future.

We plan to run the e^+ program in successive phases. In the Phase-I, a 60 GeV positron beam will be used, accumulating up to 10^{11} positrons-on-target (e^+OT). A $\simeq 30$ GeV missing energy threshold will allow us to explore the A' mass region between 175 and 250 MeV. In the Phase-II, we will further lower the positron beam energy to 40 GeV, accumulating a comparable statistics to explore the A' masses down to $\simeq 135$ MeV. These efforts will allow us to probe the LDM parameter space down to the "thermal targets" for $\alpha_D = 0.1$ and $m_{A'} = 3m_\chi$. For these measurements, we will use the existing NA64 detector at H4, whose characteristics and performances are compatible with the alleged requirements, upgrading two critical items to match them to the low-energy regime. Starting from Phase-I, a new synchrotron radiation (SR) detector will be used, to cope with the lower SR power emitted by the low-energy impinging positrons. In the second phase, also in light of the Phase I results, we plan to possibly use a new $PbWO_4$ active target, whose improved energy resolution will allow us to fully exploit the resonant missing-energy signature of the signal. Finally, based on the obtained results, we also envisage to perform further measurements, possibly also at different beam energy, to accumulate further statistics and probe the LDM "thermal targets" for different α_D and $m_{A'}/m_\chi$ values, as well as to explore different beyond SM scenarios.

Contents

1 Introduction: LDM search with positrons at NA64

Numerous cosmological and astrophysical observations unequivocally indicate that 85% of the matter of our Universe is made by a new form of matter, called "Dark Matter" (DM), gravitationally interacting with the ordinary matter described by the Standard Model (SM), but not directly emitting or absorbing light [2–4]. At present, the particle content of DM is unknown. Among the different theories that have been postulated to explain the DM microscopic properties, the Light Dark Matter (LDM) hypothesis assumes that DM is made by sub-GeV particles, interacting with SM particles through a new force. LDM particles (here denoted as χ) can be the lightest stable states of a new "Dark Sector" (DS) in Nature, with its own particles and fields.

A representative LDM model involves the existence of a new $U(1)_D$ hidden symmetry in Nature, associated to a massive gauge boson, also called "dark photon" (A'). The dark photon can kinetically mix with the ordinary photon, thus acting as a "portal" between the DS and the SM [5, 6]. In this framework, the new Lagrangian term extending the SM, omitting the LDM mass term, reads:

$$\mathcal{L} \supset -\frac{1}{4}F'_{\mu\nu}F'^{\mu\nu} + \frac{1}{2}m^2_{A'}A'_{\mu}A'^{\mu} - \frac{\varepsilon}{2}F_{\mu\nu}F'^{\mu\nu} - g_D A'_{\mu}J^{\mu}_D \tag{1.1}$$

where $m_{A'}$ is the dark photon mass, $F'_{\mu\nu} \equiv \partial_\mu A'_\nu - \partial_\nu A'_\mu$ is the dark photon field strength, $F_{\mu\nu}$ is the SM electromagnetic field strength, $g_D \equiv \sqrt{4\pi\alpha_D}$ is the dark gauge coupling, J^μ_D is the LDM current under $U(1)_D$, and ε parametrizes the degree of kinetic mixing. While it is reasonable to assume that $g_D \sim 1$, the range $\sim 10^{-4} - 10^{-2}$ ($\sim 10^{-6} - 10^{-3}$) is predicted for ε, if the kinetic mixing could generated in "Grand Unified Theories" at the one (two)-loop level [7–9]. Cosmological arguments connected to the DM thermal origin in the early Universe provide a relation between the measured DM relic density and the model parameters:

$$y \equiv \alpha_D \varepsilon^2 \left(\frac{m_\chi}{m_{A'}}\right)^4 \rightarrow y_{min} \simeq f \cdot 2 \cdot 10^{-14} \left(\frac{m_\chi}{1\,\mathrm{MeV}}\right)^2 \quad , \tag{1.2}$$

where $f \sim 1$ is a dimensionless quantity that depends on model specific details such as the LDM quantum numbers and the $m_{A'}/m_\chi$ ratio. For a given value of m_χ, it follows from Eq. 1.2 that there is a *minimum value* of y that experiments can probe, resulting in a clear, predictive target to confirm or rule out the LDM theory [10].

Experimental searches with accelerators at moderate beam energies (10 GeV – 100 GeV) have a unique discovery potential in a broad range of the LDM parameter space. Operating in the relativistic regime, these efforts do not pay any kinematic penalty for the detection of low-mass DM, and similarly do not suffer from the form-factor induced cross section suppression that characterizes specific LDM models. For a full review on current and future measurements, see e.g. Ref. [10–15].

Among all experimental techniques, missing-energy experiments have an enhanced sensitivity to the signal for the *invisible decay* scenario ($m_{A'} > 2m_\chi$), since, by measuring the prompt A' production without detecting the invisible LDM decay products, the expected

signal yield scales as ε^2, compared to the ε^4 dependency of beam-dump experiments. In this approach, the LDM production signature consists in a large *missing energy* i.e. the difference between the nominal beam energy and that one deposited in a hermetic active target, evaluated event-by-event [16]. For an electron/positron beam setup, two reaction mechanisms are relevant, the radiative and the resonant A' production [17, 18]. In particular, the second channel, in which a positron – either the primary or a secondary one – annihilates with an atomic electron producing a $\chi\chi$ pair via the A' $s-$channel exchange, ($e^+e^- \to A' \to \chi\chi$) allows to explore the large-mass A' region ($m_{A'} \gtrsim 100$ MeV). Indeed, the A' radiative production by a high-energy e^+/e^- on a heavy nuclei scales as $1/m^2_{A'}$, and it is further suppressed at large dark photon mass due to the loss of nuclear coherence and the reduction of the Weizsacker-Williams effective photon flux [19]. On the other side, for a narrow A' ($\alpha_D \lesssim 0.1$), the annihilation cross section σ_{res} at the resonance peak reads

$$\sigma^P_{res} = \frac{1}{\Gamma}\frac{4\pi\alpha_{EM}\epsilon^2}{m_{A'}} \quad , \tag{1.3}$$

where Γ is the total width (a complete description of the resonant cross section is presented in App. A). It follows that, for $m_{A'}$ values within the kinematic region accessible by the missing-energy measurement, the total signal yield, obtained by integrating this cross section over the positrons track-length distribution $T(E_+)$, scales as $N_S \simeq \Gamma\sigma^P_{res}T(E_R) \propto T(E_R)/m_{A'}$, where $E_R = m^2_{A'}/(2m_e)$ is the resonant energy. For an *electron-beam* missing-energy measurement, thanks to the secondary positrons of the electromagnetic shower, this mechanisms leads to a sensitivity improvement for $E_R \simeq E^{thr}_{miss}$ with a reduction for $E_R \to E_0$ due to the $T(E_+)$ suppression[1]. Recently, the NA64 results from the 2016-2018 runs have been re-analyzed to include this signal production channel, obtaining an improvement of the exclusion limits in the 200-300 MeV region by almost an order of magnitude, touching for the first time the dark matter relic density predicted parameter combinations [20] (see also Fig. 1, right panel).

For a *positron-beam* measurement, instead, thanks to the $T(E_+)$ enhancement for $E_+ \to E_0$ associated to the primary positron, no signal suppression is present; the sensitivity to ε is almost flat for all accessible A' masses, roughly corresponding to the range $\sqrt{2m_eE^{thr}_{miss}} \div \sqrt{2m_eE_0}$, ignoring for simplicity the suppressed contribution of the off-shell A' production. **This motivates a multi-energy experimental program with a positron beam, allowing to fully exploit the peculiarities of the resonant A' production to "scan" the LDM parameter space for $m_{A'} \gtrsim 100$ MeV.**

The NA64 experiment at CERN SPS provides the natural environment for such an experimental effort. This new measurement is based on the use of a positron beam impinging on the NA64 active thick target to search for LDM produced via the resonant annihilation of the primary positron and its secondaries with atomic electrons. Specifically, we propose to run a dual-phase measurement, with the first (second) phase running at 60 (40) GeV beam energy. Assuming conservatively a 50% missing energy threshold, with 10^{11} accumulated

[1] Here, E_0 is the primary beam energy and E^{thr}_{miss} the missing energy threshold.

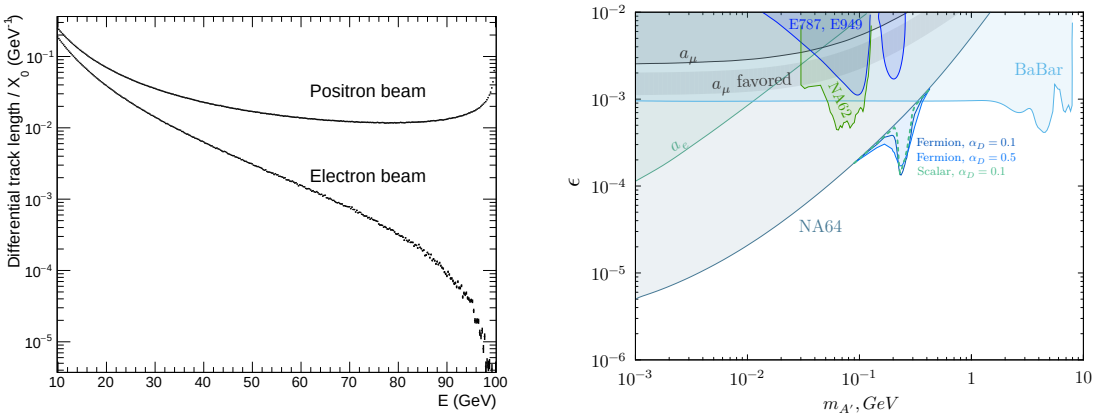

Figure 1. Left: differential positrons track-length distribution in a thick target for an impinging 100 GeV e^-/e^+ beam, normalized to the radiation length X_0.
Right: the latest NA64 exclusion limit for invisibly-decaying dark photons [21]. Existing limits from BaBar [22], E787 and E949 [23], and NA62 [24] are shown, as well as the favored area from the muon $g-2$ anomaly [25, 26]. The continuous blue line report the previous NA64 result, without including the contribution from e^+e^- annihilation. The three lines labeled with "Fermion, $\alpha_D = 1$", "Fermion, $\alpha_D = 0.5$", and "Scalar, and $\alpha_D = 0.1$" correspond to the exclusion limit obtained by also considering the resonant contribution from the annihilation channel, for different parameters of the LDM model (α_D value and LDM quantum numbers).

e^+OT for each configuration, this effort will explore the LDM parameters space down to the "thermal target" for 140 MeV $\lesssim m_{A'} \lesssim$ 250 MeV.

We underline that the proposed effort is fully complementary to the main NA64 electron-beam missing-energy search, already approved by CERN SPSC. Indeed, each of the two programs (electron-beam and positron-beam) is optimized to explore a specific mass range. This dual approach empowers NA64 to emerge as a unique experiment, poised to either unveil or definitively refute the LDM hypothesis across a broad A' mass range in the near future. We also stress that the possibility to run the e^+ measurement using the existing NA64 detector, with restricted upgrades only for selected sub-components, makes this program very cost effective. Finally, the possibility to easily and quickly re-configure the e^+/e^- H4 beam for different energies or polarity will permit to run the positron measurement just after a NA64 electron run, resulting in an optimized use of the beam-time.

2 Summary of the 100 GeV test

A first pilot measurement was performed in summer 2022 using a 100 GeV positron beam impinging on the existing NA64 detector, sketched schematically in Fig. 2 (for more details see Sec. 3.2). The total accumulated statistics was $\simeq 10^{10}$ e^+OT [1]. The main goal of this measurement was to demonstrate, for the first time, the validity of the positron-beam missing-energy technique to search for LDM, identifying the corresponding critical items and determining an appropriate strategy to mitigate them, in view of the future

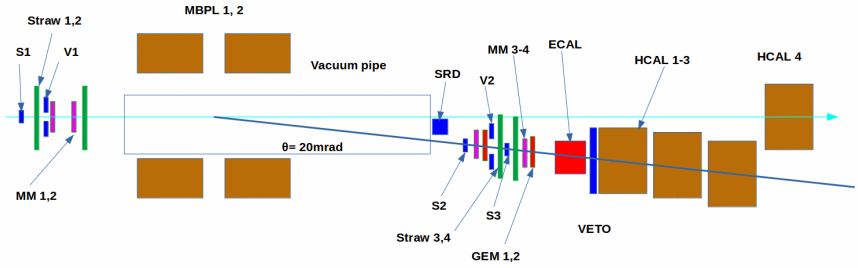

Figure 2. Schematic illustration of the NA64 2022 setup to search for invisible decays of the A's resonantly produced by the annihilation of the 100 GeV impinging e^+ with the atomic electrons of the active ECAL target.

e^+ program. During this measurement, we reversed the H4 beamline optics, obtaining a $E_0 = 100$ GeV e^+ beam, and we searched for high missing-energy (> 50 GeV) events compatible with the LDM particle production.

As described in Sec. 3.1, the hadron contamination affecting the positron beam at 100 GeV is higher than that for the electron beam (see also the detailed study in Ref. [27]). Consequently, to not overcome the maximum DAQ system acquisition rate, we set the ECAL missing energy trigger threshold to ~ 55 GeV, unavoidably limiting the extension of the side-band region $E_{ECAL} < E_0$, $E_{HCAL} = 0$ employed for the background yield extrapolation. In addition, we set the trigger energy threshold for the ECAL preshower (ECAL0) at ~ 400 MeV. The effect of this choice on the signal yield is visible in the left panel of Fig. 3, reporting the corresponding efficiency as a function of the ECAL0 threshold for different $M_{A'}$ values ($\alpha_D = 0.5$). In all cases, the efficiency variation for the ECAL0 threshold in the range 300-600 MeV is less than 10%. The most significant effect is observed for larger $M_{A'}$ values since, for $M_{A'} \simeq 300$ MeV (350 MeV), the positron resonant energy for the process $e^+e^- \to A' \to \chi\overline{\chi}$ is approximately 88 GeV (120 GeV), close to the beam energy. Consequently, the production process occurs within the first few radiation lengths of the ECAL, when the energy of the primary positron has not yet degraded significantly, and the electromagnetic shower has not yet developed. Therefore, only limited energy is released in the preshower, and the corresponding energy threshold is not satisfied. In conclusion, to increase the signal yield and decrease its dependence on $M_{A'}$, it is necessary to reduce the preshower trigger threshold as much as possible: for future positron measurements an ad-hoc optimization study will be thus needed.

In this measurement, we adopted a blind analysis approach, maximising the signal efficiency for the A' resonant production channel. The adopted selection cuts required the presence of an incoming track with momentum $P_0 \sim 100$ GeV/c, tagged as a positron by the SRD. Additionally, we selected events in which the shape of the electromagnetic shower in the ECAL was consistent with the expected signal profile for A', and with null activity in the downstream detectors (VETO and HCAL). We estimated the signal yield via a GEANT4-based simulation of the NA64 setup using the DMG4 package [28], applying to Monte Carlo events the same selection cuts used in the data analysis. To validate the MC simulations, and to optimize the shower-shape cut, we exploited the so-called "di-

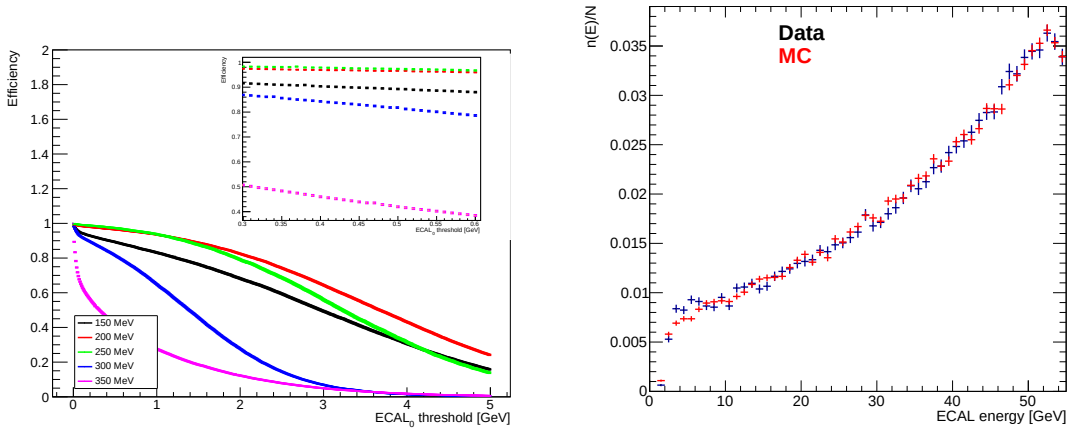

Figure 3. Left: The A' signal efficiency as a function of the ECAL0 energy threshold, for different dark photon masses; the inset reports a zoom in the 300-600 MeV region. Right: ECAL energy distribution of di-muon events from data (black) and from MC (red). Both distributions are normalized to unity in the energy interval $[0, 55]$ GeV.

muon" events. In these events, a high-energy $\mu^+\mu^-$ pair is produced in the ECAL through radiative production (conversion of a Bremsstrahlung photon in the EM field of a nucleus, $\gamma N \to \mu^+\mu^- N$) or atomic annihilation production ($e^+e^- \to \mu^+\mu^-$). These "di-muons", characterized by the MIP (minimum ionizing particle) nature of high-energy muons, exhibit a topology similar to the signal events and can be thus used as a benchmark for the analysis. In the analysis, we selected di-muon events by applying a cut on the deposited energy in the HCAL modules, and we asked for a clean 100 GeV/c impinging positron track. The normalized ECAL energy distribution for the measured di-muon events is reported in Fig. 3 right panel, compared to the MC prediction. A good agreement is observed. In particular, the annihilation channel contributes to events with large missing-energy (low ECAL energy), representative of the $m_{A'}$ range where the expected sensitivity is higher[2] - this is a remarkable difference with respect to the electron beam case, where this channel is negligible.

Due to the high hadronic contamination, the most significant background contribution arises from the upstream decay $K^+ \to e^+\pi^0\nu_e$ of misidentified kaon contaminants. If the produced neutrino energy exceeds 50 GeV and the $e^+\gamma\gamma$ particles produce a single low-energy electromagnetic shower in the calorimeter, this decay leads to a background. Similarly, a minor contribution originates from the branching-ratio suppressed $\pi^+ \to e^+\nu_e$ decay. The second most significant background channel involves upstream hadron production through the e^+ interaction with the beamline materials [16]. In this case, the low-energy positron impinges on the target while one or more high-energy neutral hadrons are emitted forward and escape detection [29]. We estimated this contribution using the larger dataset collected by NA64 in 2022 with a 100 GeV e^- beam, employing the same detector configuration and reversed beamline optics. We performed a dedicated Monte Carlo comparison to ensure that the differences between electron and positron hadron

[2]The annihilation production channel had to be explicitly included in the Monte Carlo simulations.

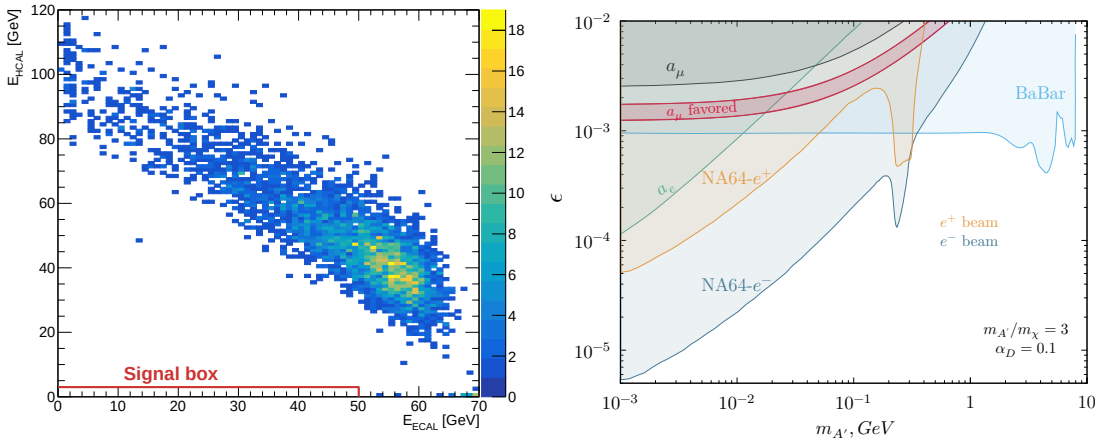

Figure 4. Left: The HCAL vs ECAL energy distribution for events satisfying all analysis cuts. The signal region is also reported (for better visualization, it has been expanded by a factor $\times 3$ along the vertical axis). Right: The obtained sensitivity (orange curve) in the ε vs $m_{A'}$ space for the 100 GeV positron-beam test performed. The most stringent LDM exclusion limits from BaBar [22] and NA64 [21] are also shown, as well as the favored area from the muon $g-2$ anomaly [26, 30] (red lines).

production are negligible. Combining all the contributions, a total background yield of $B = (0.09 \pm 0.03)$ events was obtained. This result shows the detector's capability to detect and reject hadron-induced background events at 100 GeV e^+ beam energy. Since at lower beam energies the hadronic contamination significantly decreases (see Sec. 3.1), we expect this background channel to be suppressed, thus further supporting the idea of exploring the low A' mass region using the NA64 missing-energy approach.

After unblinding the data, no events were observed in the signal region, defined as $E_{ECAL} < 50$ GeV and $E_{HCAL} < 1$ GeV, as reported in Fig. 4. Based on this result, we derived an upper limit on the coupling parameter ε of the A' particle as a function of its mass $m_{A'}$. The obtained exclusion limit is reported in Fig. 4 for fermionic LDM, with $\alpha_D = 0.1$ and $m_{A'} = 3m_\chi$. In conclusion, we performed the first positron-beam missing-energy measurement searching for LDM, exploiting the existing NA64 setup. The resulting limits touch the latest NA64 electron-beam results corresponding to a $\sim$2 orders of magnitude larger electron statistics: this proves the feasibility and the potential of a dedicated effort with positron beams at the CERN H4 beamline.

3 Proposed experimental setup

The remarkable results of the pilot experiment demonstrate the potential of a dedicated effort with positron beams. Therefore we propose a dual-phase positron-beam missing-energy measurement performed with the NA64 experiment at CERN SPS. The measurements will make use of the positron beam from the H4 beamline impinging on the NA64 active thick target. LDM particles will be mainly pair-produced via the resonant annihilation of the primary and secondary positrons with atomic electrons ($e^+e^- \to A' \to \chi\overline{\chi}$). The specific

signature for signal events will be a well-defined value of the missing energy measured in the active target, depending only on the dark photon mass.

The Phase-I will exploit the 60 GeV positron beam and accumulate up to 10^{11} e^+OT. Considering a missing energy threshold equal to half of the beam energy, the Phase-I measurement will scan the A' mass region between 175 and 250 MeV. In order to be sensitive to lower A' mass values, in the Phase-II we will perform a measurement using a 40 GeV positron beam accumulating statistics comparable to the first phase. Therefore, we will explore the A' masses down to 140 MeV. We aim to perform the measurements using the existing NA64 detector at H4. However, the low-energy regime requires specific detector upgrades concerning the SRD and ECAL sub-detectors. During operation, the ECAL energy threshold in the main trigger will be adjusted to not exceed the DAQ rate capability and, at the same time, permit to record events with the lowest missing energy possible. The following approach to the data analysis will be adopted. First, events in the signal region, based on a preliminary choice of the ECAL and HCAL energy cuts, will be excluded from the analysis. Then, the expected number of background events will be evaluated using both Monte Carlo simulations and data-drivern extrapolations from the events measured in the control region, in order to set the optimal selection cuts that maximize the experiment sensitivity. Finally, the signal region will be scrutinized.

3.1 The e^+ beam at the H4 beamline

The H4 beamline at the CERN North Area facility is a versatile beamline capable of transporting high-energy particles with momentum in the range of 10-400 GeV/c, with variable composition and purity. The beam is obtained by having a primary 400 GeV/c proton beam from the SPS impinging on a thin beryllium target (T2), and then selecting secondary or tertiary particles through a set of magnets and beam absorbers/attenuators [31, 32]. The particles produced at the target are momentum-selected and transported through a $\simeq$ 600-m long beamline, composed of several bending dipoles, focusing quadrupole, and corrector elements towards the experimental area. Collimating structures and beam instrumentation are also present and used to ensure the beam properties on a spill-by-spill basis. When operated in electron/positron mode, particles are produced via a dual conversion process, by having the decay photons from π^0/η mesons produced in the T2 target propagating downstream at zero production angle and pair-converting on a thin lead secondary target. A magnetic field between the two targets sweeps away all secondary charged particles produced in the T2 target and deflects away the primary proton beam. After the converter, at the start of the H4 beamline, a septum magnet is used to perform a first momentum and charge sign selection of the particles that are transported to the experimental area.

The purity of the positron beam is a critical parameter for the measurement, since contaminating hadrons are a dominant source of background events, as discussed in Sec. 4. In particular, an upstream in-flight decay of an impinging hadron to a final state involving a soft electron and an energetic neutrino can mimic the signal signature. The value of the hadronic contamination also reflects on the experiment trigger configuration. Impinging hadrons typically deposit only a limited fraction of the primary beam energy in the ECAL, thus satisfying the missing-energy trigger condition. A detailed knowledge of the hadronic

contamination is thus required to tune the trigger threshold parameter, directly reflecting to the experiment sensitivity.

In the electron/positron configuration, the main source of hadron contaminants in the beam is the forward production of long-lived neutral particles in the target, such as Λ hyperons and K_S, propagating downstream and decaying to charged particles after the sweeping magnet. When the beamline is operated in negative-charge mode (e^-), the contamination in the low momentum range, $P \lesssim 100$ GeV/c, is mostly due to the pions from $\Lambda \to p\pi^-$ decay. At larger momentum this contribution drops because of the kinematic limit of the decay process[3], and the main source of hadron contaminants is the K_S decay to a $\pi^+\pi^-$ pair. In positive-charge mode (e^+), instead, there is no kinematic suppression at large momentum for the protons from Λ decay. Therefore, a larger intrinsic hadronic contamination of the beam is expected with respect to the electrons one. This effect is illustrated in Fig. 5, showing the H4 beam hadrons-to-electrons (h/e) ratio as a function of the energy in the negative-charge (black) and positive-charge (red) mode, as obtained from a FLUKA-based simulation. This simulation was validated through a dedicated measurement performed at 100 GeV, as discussed in Ref. [27], finding a very good agreement.

A key element for the proposed measurement is the observation that the hadronic contaminant fraction in the beam wanes strongly at decreasing beam energy. This strongly reduces the contribution of hadron-induced background events less critical, simultaneously allowing to use a lower ECAL missing energy threshold, thus increasing the experiment sensitivity[4]

3.2 The NA64 detector

The detector currently used for the NA64 program at the H4 beamline has three main sections: the "upstream" part, responsible for the tagging of the incoming particles of the beam, the active target, where the impinging particles are degraded and their energy deposition is measured and, finally, a "downstream" section, aimed to detect penetrating SM particles (muons, neutrons...) exiting the active target (see also Fig. 6). More specifically, impinging particles are detected by a set of three plastic scintillator counters (SC) and a veto counter V_1. Their momentum is measured by a magnetic spectrometer, composed of a set of tracking detectors (GEMs, MicroMegas, and Straw tubes) installed upstream and downstream a dual dipole magnet with total magnetic strength $\int Bdl \simeq 7$ T$\cdot$ m. The momentum resolution $\delta p/p$ is $\simeq 1\%$. Particle identification is achieved by measuring the synchrotron radiation emitted by the particles deflected by the magnetic field through a compact Pb/Sc calorimeter (SRD). The NA64 active target is a $40X_0$ Pb/Sc

[3]Starting from a $P_0 = 400$ GeV/c proton beam, the maximum energy of the π^- from the decay of a Λ baryon produced in the Be target is $E^{\pi}_{max} \simeq \frac{P_0}{M_\Lambda} \cdot (E^*_\pi + P^*_\pi)$, where E^*_π (P^*_π) is the pion energy (momentum) in the Λ rest frame. Numerically, $E^{\pi}_{max} \simeq 97$ GeV. The proton maximum energy is $E^{p}_{max} \simeq 375$ GeV. For comparison, the maximum pion energy from the $K_s \to \pi^+\pi^-$ decay is $E^{\pi}_{max} \simeq \frac{P_0}{M_K}(E^*_\pi + P^*_\pi)$. Numerically, $E^{\pi}_{max} \simeq 366$ GeV.

[4]As anticipated before, in this document we conservatively consider a missing-energy threshold equal to half of the beam energy.

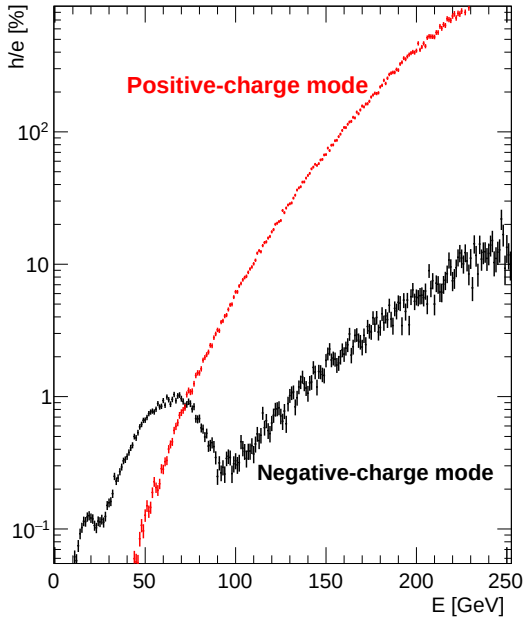

Figure 5. The ratio h/e between hadrons and electrons / positrons at the H4 lead converter, predicted by Montecarlo. The angular and momentum acceptance of the H4 beamline have been applied both for the negative-charge (black) and positive-charge (red) modes. The structure at $E \simeq 50$ GeV for the negative charge mode is the result of the convolution between the energy spectrum of the produced Λ baryons and the maximum energy allowed in the $\Lambda \to p\pi^-$ decay.

in-homogeneous calorimeter (ECAL), assembled as a 5×6 matrix of 5×5 cm^2 cells with independent PMT readout. The calorimeter is segmented into a $4X_0$ pre-shower section (ECAL0) and a main section (ECAL1), allowing to measure the longitudinal shower development. The ECAL energy resolution is $\sigma_E/E \simeq 10\%/\sqrt{E(\mathrm{GeV})} + 4\%$. In 2022, a new hadronic calorimeter veto (VHCAL) was added upstream of the ECAL. This detector, a Cu-Sc hollow calorimeter, serves as an efficient veto against upstream electroproduction of large-angle hadrons. The downstream section of the detector is composed of a hermetic Fe/Sc hadron calorimeter (HCAL) and a high-efficiency plastic scintillator counter (VETO). Three HCAL modules (HCAL0, HCAL1, HCAL2), each with length $\simeq 7\lambda_I$ and transverse size $\simeq 60 \times 60$ cm^2, are installed downstream of the ECAL, in order to detect secondary hadrons and muons produced by the interaction of the primary beam with the target or with others upstream detector elements. The VETO detector is installed between the ECAL and the HCAL to further suppress the background due to muons and other charged particles produced in the ECAL. A fourth HCAL module (HCAL3) is installed at zero degrees, aligned to the undeflected beam direction, to catch neutral particles produced by the beam interaction with upstream beamline materials.

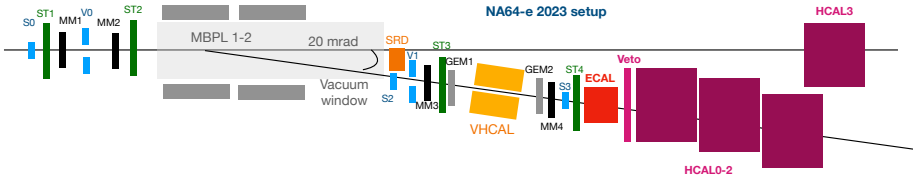

Figure 6. Schematic setup of the NA64 detector (2023 run).

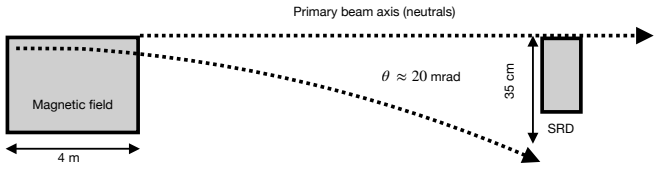

Figure 7. The NA64 dipole magnet (grey box on the left) and the Synchrotron Radiation Detector (grey box on the right). The dashed lines identify the primary beam axis, where neutral particles proceed without being deviated by the magnetic field, and the extremity of the deflection plane of the charged particles. The vertical arrow near the SRD identifies the overall area of impact of the photons, of which the SRD covers just a fraction.

3.3 New experimental equipment

3.3.1 The Synchrotron Radiation Detector

As mentioned in Sec. 3.2, the NA64 experiment exploits the synchrotron radiation emission of the impinging electrons/positrons within the upstream magnetic field to identify them, thus allowing to reject contaminants in the beam [33]. An overview of the current NA64 SRD is illustrated in Fig. 7. By passing through the magnet, the impinging 100 GeV e^- is deflected by an angle of approximately 20 mrad, resulting in the average emission of 40 photons, with a mean energy of 3.8 MeV. The photons are emitted uniformly along the path of the deflected e^- in the bending plane, with a trajectory approximately collinear with the beam trajectory. After the magnet, a 10-meters-long vacuum pipe is installed. In the position where the SRD is located, the extension of the photon impinging arc is ∼35 cm. The current SRD detector is an inhomogeneus calorimeter composed of alternating layers of lead and scintillator, i.e. 100 layers with 0.01-cm-thick lead sheets and 0.11-cm-thick scintillator sheets, and further 100 layers with 0.018-cm-thick lead and 0.11-cm-thick scintillator sheets. All layers are crossed by optical fibers, collecting scintillation light and conveying it to photomultiplier tubes (PMT). This geometry was optimized for the detection of the synchrotron radiation emitted by 100 GeV e^- in the NA64 dipole magnetic field.

To verify if the performance of the current detector is adequate for the proposed measurements, Monte Carlo simulations at different beam energies were carried out; the results are reported in Fig. 8. As expected, the energy deposition is significantly reduced in the cases of our interest, 60 GeV and 40 GeV: the emitted synchrotron radiation is in fact proportional to the fourth power of the impinging particle energy [34]. Such low-energy emission result in few photons detected by the PMTs and, therefore, in a low detection

efficiency for a $\simeq$ MeV detection threshold. We are thus examining two possible alternative solutions: the modification of the geometry of the current detector, in order to maximize the energy deposited in the active material by increasing the number of detected photo-electrons, and a new detector layout based on LYSO/LSO crystals.

We emphasize that the goal of the study was to identify a possible SRD detector design optimized for low-energy SR photons, whose performance matches the requirements of the positron-beam measurement in terms of of efficiency and rate of false-positives, in order to demonstrate the feasibility of the low-energy positron-beam measurements. The specific detector design will be defined during LS3, based on the R&D measurements that will be performed during the next two years (see also Sec. 6.1).

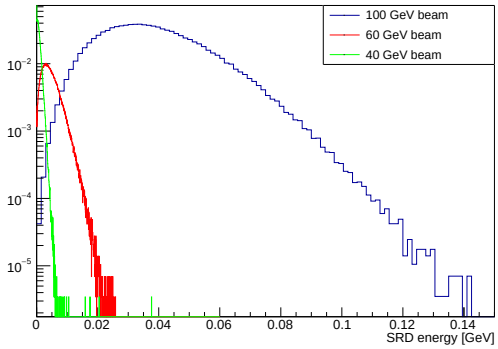

Figure 8. Monte Carlo simulations for the NA64 SRD detector at different beam energies. The distribution at 60 (40) GeV is peaked at 0.8 (0.2) MeV.

Optimization of the current design A possible solution is an SRD detector based on the same Pb/Sc technology, but bearing an optimized thickness ratio between lead and plastic to increase the deposited energy on the active material, and thus the light collected by the PMTs. A Monte Carlo simulation was conducted to verify if the thickness variation of the layers could lead to a significantly larger light collection, thus determining easily identifiable signals for the beam energies discussed in this document. Results are reported in Fig. 9. The spectrum of the energy deposited in the case of the standard geometry (reported in Sec. 3.3.1) is shown in blue. Red and green curves represent the energy spectra of geometries A and B, defined as follows.

- **Geometry A** The thickness of the lead sheets is halved, and the number of layers of both materials increased: 200 layers with lead thickness of 0.005 cm and 200 layers with 0.009-cm-thick lead sheets;
- **Geometry B** The thickness of the lead sheets is reduced to a quarter of the standard configuration. Again, the number of layers of both materials is increased: 400 layers with a lead thickness of 0.0025 cm and 400 layers with 0.0045 cm-thick lead sheets.

In both optimized geometries the layers number has been increased to maintain an overall lead thickness equal to 2.8 cm (5 radiation lengths). The thickness of the plastic scintillator

sheets is left unchanged (0.11 cm). By reducing the thickness of the lead sheets and increasing the overall number of layers, the peak of the deposited energy in the scintillator moves towards higher values: at 60 GeV the deposited-energy distribution shows a peak at 2.8 MeV for the standard SRD configuration, at 4.5 MeV for geometry A and 5.5 MeV for geometry B; at 40 GeV, the deposited energy is peaked at 300 keV in the standard configuration, at 400 keV for geometry A and, finally, at 700 keV for geometry B.

In conclusion, for both beam energy values, the deposited energy in the active material increases by a factor $\approx$ 1.5 (2) in configuration A (B). Assuming therefore to double the energy deposited in the active material, the light detected by the PMTs would be proportionally doubled.

New design based on LYSO crystals LYSO ($Lu_{2(1-x)}Y_{2x}SiO_5$) crystals are characterized by a good light yield ($LY \approx 3 \cdot 10^4$ ph/MeV [35]), high density, and short decay time (about 40 nanoseconds) [36], making it an optimal candidate to detect SR photons. In order to study the feasibility of the new approach, we considered a *preliminary LYSO-based SRD design* based on crystals with a face size of 2×2 cm^2 and a length of 5 cm, assembled in a 14×5 matrix, the length of the crystals being perpendicular to the bending plane, as schematized in Fig. 10. The light readout is performed through SiPMs with a face area of 6x6 mm^2 and a pixel size of 25x25 μm^2 (model MPPC S13360 by Hamamatsu). In the aforementioned configuration, we estimated the total energy deposition in the LYSO crystals ($\overline{E}_{dep}$) for the different beam energies:

$$\overline{E}_{dep} = N_\gamma \cdot G_{acc} \cdot P \cdot \overline{E}_\gamma, \tag{3.1}$$

where N_γ is the mean number of emitted synchrotron photons, $\overline{E}_\gamma$ is their mean energy, G_{acc} is a geometrical acceptance factor taking into account the difference between the detector extension and the photons impinging area ($G_{acc} \simeq 0.71$), and finally P is the photons interaction probability with the crystals. The average number of detected photoelectrons per MeV n_{phe^-} is, for each crystal:

$$n_{phe^-} = LY \cdot \frac{1}{2} \cdot \eta_{geom} \cdot \epsilon_{qu}(\lambda = 420\,nm) \simeq 470\ \text{MeV}^{-1}. \tag{3.2}$$

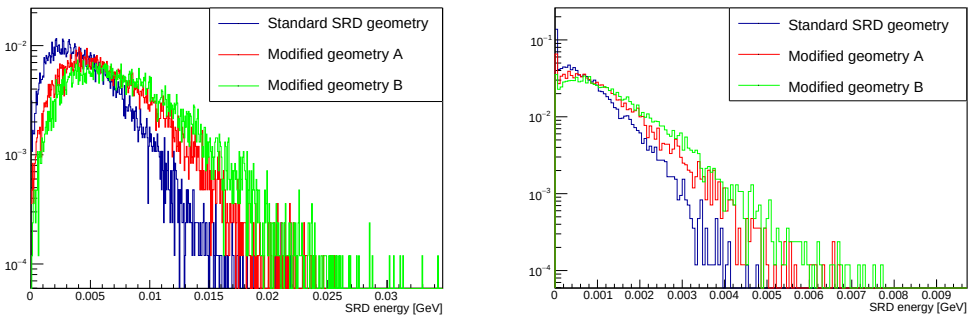

Figure 9. Results of the Monte Carlo simulations for the thickness optimization of the lead-scintillator layers of the SRD, for a 60 GeV (left plot) and 40 GeV (right plot) beam energy.

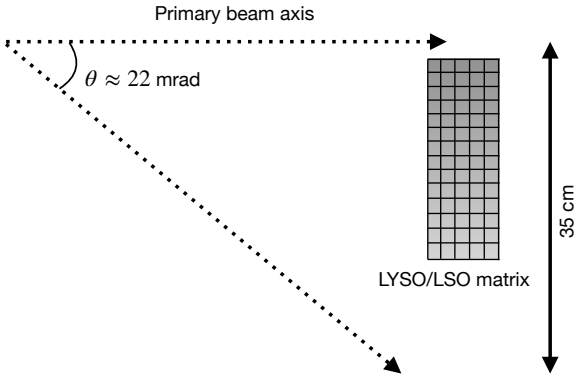

Figure 10. Overview of the LYSO matrix in the NA64 beamline.

Beam energy [GeV]	N_γ	$\overline{E}_\gamma$ [MeV]	N_γ^{det}	$\overline{E}_{dep}$ [MeV]	N_{phe}^{crs}
100	40	3.8	25	95	1026
60	25	0.8	19	15.2	216
40	16	0.24	12	2.9	65

Table 1. Estimate of the average number of emitted synchrotron photons for each impinging positron N_γ, the average energy for single synchrotron radiation photon $\overline{E}_\gamma$, the average number of synchrotron radiation photons actually interacting with the LYSO crystals N_γ^{det}, the average total energy deposited in the detector $\overline{E}_{dep}$ for each event, and the typical number of photo-electrons detected per crystal N_{phe}^{crs}.

Here, LY is the typical light yield of LYSO crystals ($\approx 3 \cdot 10^4$ photons/MeV), $\frac{1}{2}$ is a conservative factor assuming that only half of the photons are detected by the photosensors, η_{geom} is the ratio between the area of the SiPMs (6×6 mm^2) and the area of each crystal's face (20×20 mm^2) and, finally, $\epsilon_{qu}(\lambda = 420\,nm)$ is the quantum efficiency of the SiPMs at a wavelength equal to 420 nm, the typical LYSO/LSO emission length ($\epsilon_{qu}(\lambda = 420) \simeq 0.2$ for Hamamatsu MPPC S13360 series). This calculation was carried out for beam energies equal to 100, 60, and 40 GeV. As shown in Tab. 1, the average number of synchrotron photons N_γ^{det} interacting with the detector is lower than the number of crystals for all the beam energy values. We therefore considered as typical energy deposition in each crystal the average energy of a single synchrotron photon ($\overline{E}_\gamma$). In order to exclude any SiPM saturation effect, we verified that the average number of photoelectrons detected per crystal was lower than the number of cells in each SiPM by at least a safety factor of 10. This requirement is satisfied for all the considered beam energies. Given the above considerations, the proposed layout with LYSO crystals appears as a good solution for a new SRD detector allowing particle identification at the beam energies considered in this document.

To further study and validate this solution, we carried out dedicated Monte Carlo simulations, implementing the new detector description within the NA64 simulation framework.

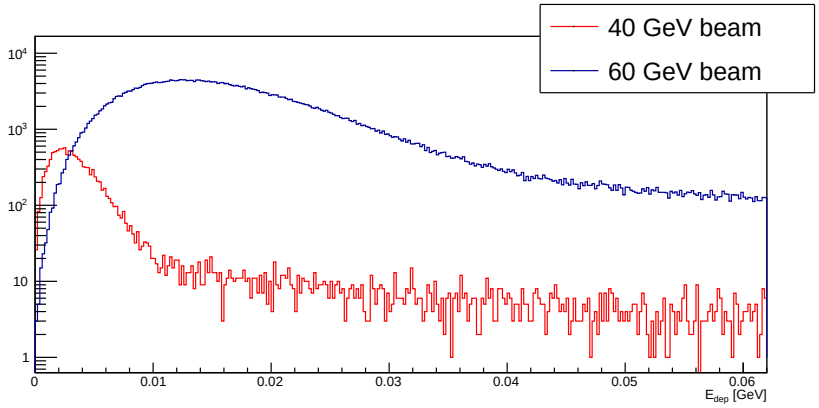

Figure 11. Distribution of the deposited energy in the SRD with a 60 (40) GeV positron beam in blue (red).

The results are shown in Fig. 11, reporting the total energy deposited by SR photons in the SRD. At 40 (60) GeV beam energy the deposited energy distribution is peaked at 3.5 (12) MeV, in good agreement with the analytical estimates previously discussed. To obtain an estimate of the detector's positron identification efficiency, two thresholds were set, the first being in terms of energy deposited on the individual crystals for each event, and the second on the number of crystals in which the energy threshold is exceeded for each event (referred in the following as "multiplicity"). This second condition was introduced mainly to suppress false-positive events due to the intrinsic LYSO radioactivity, since events induced by Lu decay typically result to energy deposition in a single crystal (see also Appendix B.2).

For an energy threshold value equal to 100 phe and multiplicity equal to 2 an efficiency of 0.888 (0.999) was found for a 40 (60) GeV beam. We also checked the effect of different detector geometries, reducing the number of crystals in the matrix to simplify the overall detector design, in light of the short mean free path of MeV photons in this material [37]. The results obtained by removing some crystal rows (so, passing from a 14×5 to a 14×1 matrix) are shown in Fig. 12, reporting the total energy deposited in the detector by SR photons emitted by a 40-GeV e^+ beam. The blue, red, and green distributions appear identical, suggesting the validity of the 14×3-matrix design for the detector. There is a slight change in the energy deposition for the magenta distribution, while the cyan distribution shows a significantly lower mean energy. As for the efficiency, it goes from 0.888 for the 14×5 geometry to 0.887 for the 14×4 geometry to 0.886 for the 14×3 geometry.

Finally, we evaluated the probability of "false positive" effects, induced both by the intrinsic radioactivity of the crystals associated with the decay of ^{176}Lu or by afterglow effects. Afterglow effects – also referred to as "afterpulses" – consist in the emission of scintillation light at a much later time following a primary crystal excitation. For NA64, this scenario may result in false-positive events when a high amount of energy is deposited in LYSO crystals by a $\delta-$ray emitted from an incoming contaminant hadron. If the subsequent emission of afterglow photons coincides with the passage of another hadron, it can lead to misidentification. While the first hadron could be correctly identified due to significantly

higher energy deposition in the SRD compared to that anticipated for a positron, the second one would be misidentified. To study this phenomenon, a first preliminary test was conducted on an 8×8 matrix of LYSO/LSO crystals of 3×3×25 mm^3, which was exposed to a 160 GeV muon beam. During this test, $\simeq$ 8000 muon events were collected, of which only 0.17% gave rise to afterpulse events (for details of this test and data analysis see the Appendix B.1).

Intrinsic radioactivity can also produce a background, if a ^{176}Lu decay resulting in an energy deposition sufficient to mimic a SRD signal occurs in coincidence with the passage of a contaminating hadron [34]. To evaluate this effect, further Monte Carlo studies were carried out, simulating the random ^{176}Lu decays occurring uniformly within the LYSO matrix volume. The same cuts as for the simulations with positron beams at 40 and 60 GeV were applied to these simulations. Consequently, the rate of false-positive events (R_h) was calculated, for both the nominal configuration with 14×5 LYSO crystals and a smaller one made as a 14×3 matrix. To evaluate the absolute rate of ^{176}Lu decays, we considered the maximum ^{176}Lu number density allowed in LYSO crystals, consistent with the chemical composition $Lu_{2(1-x)}Y_{2x}SiO_5$ with $x = 0$. To evaluate the probability of a contaminating hadron crossing the detector in coincidence with false-positive SRD signal due to ^{176}Lu decays, we assumed a 50-ns coincidence window, including the effect of the SRD multiplicity threshold. The results, illustrated in Tab. 2, indicate that the rate of these possible background events is negligible (for further details, see Appendix B.2). In conclusion, from these preliminary studies we conclude that a LYSO-based SRD detector represent a promising option for measurements with low-energy positron beams.

R&D status A dedicated experimental *R&D* program is foreseen in 2024-2025 to corroborate the Monte Carlo results discussed in the previous section, in preparation to the final detector design (see also Sec. 6.1). In preparation to this, a first LYSO-based SRD detector prototype is currently being assembled by the NA64 collaboration, under the guidance and responsibility of UCF-Chile. The prototype is made of six independent modules. An exploded view of one module is shown in Fig. 13. The detector is made by a a 8×12

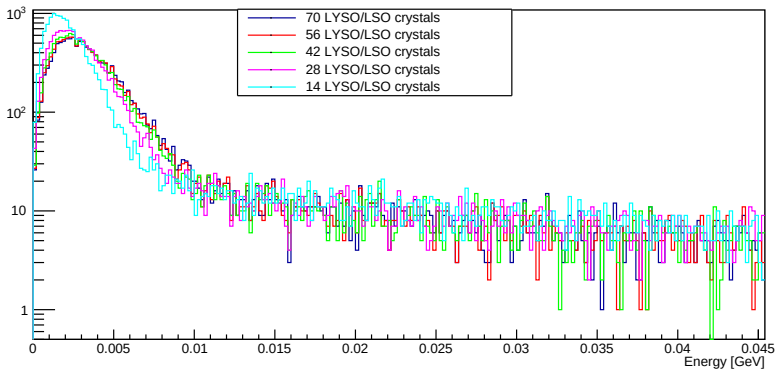

Figure 12. Energy deposited in the SRD considering a 14×5 (blue), 14×4 (red), 14×3 (green), 14×2 (magenta), and 14×1 (cyan) LYSO matrix. This simulation refers to a 40 GeV e^+ beam.

Matrix geometry	R_h at 40 GeV [Hz]	R_h at 60 GeV [Hz]
14×5	4.31	10.78
14×3	1.60	3.99

Table 2. Results of intrinsic radioactivity simulations of the LYSO in terms of hadron event rates mimicking the positron signal in the SRD. The values derived from a cut in deposited energy equal to 100 photoelectrons and multiplicity equal to 2, and were calculated taking into account the decay probability of ^{176}Lu in a coincidence window of 50 ns with the hadron and the probability of double decay in the same coincidence window.

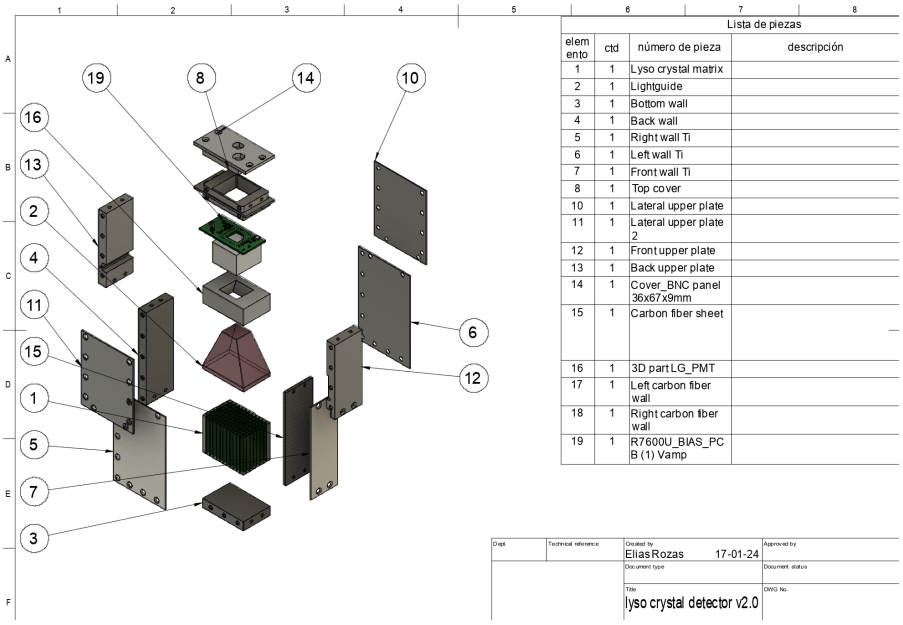

Figure 13. Exploded view of a single module of the LYSO detector prototype.

matrix of $4 \times 4 \times 45$ mm^3 LYSO crystals (n. 1 in the drawing), read by a single Hamamatsu 7600U PMT coupled to them via a light guide (n. 13 in the drawing). The matrix and the light guide are inserted in a light-tight box made by aluminum and carbon fiber plates. The response of the prototype to the SR radiation emitted by 40, 60 and 100 GeV positrons when deflected by the NA64 MBPL magnet will be measured and compared with simulations.

In parallel to this, a dedicated study is ongoing within the NA64 DAQ group to identify a strategy for the readout of SiPM signals, in particular to assess the possibility of an ASIC-based solution integrated in the NA64 DAQ system.

3.3.2 The ECAL

One of the striking features of the resonant LDM production mechanism $e^+e^- \to A' \to \chi\bar{\chi}$ is the steep cross section dependence on the energy of the incoming positron E_{e^+}. Given the resonant nature of the process, the cross section features a peak at $E_{e^+} = \frac{m^2_{A'}}{m^2_e}$ and

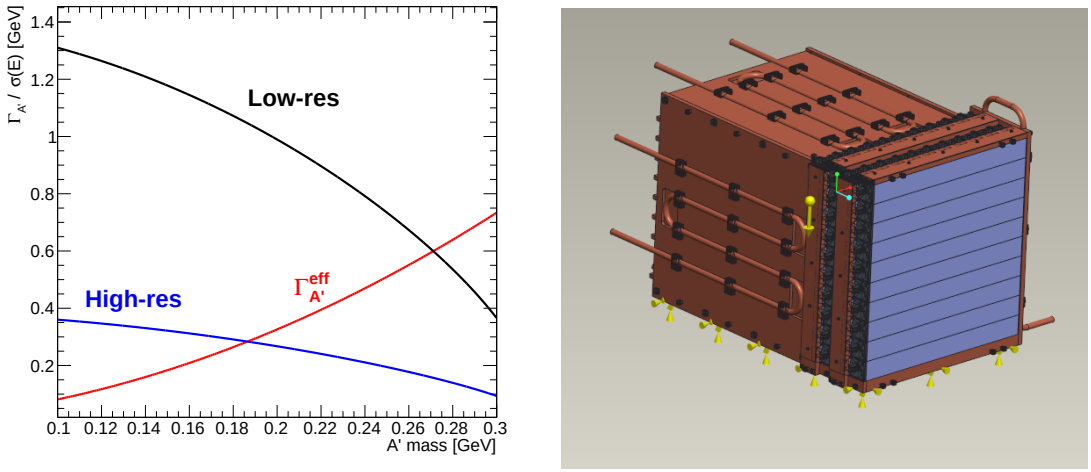

Figure 14. Left: The dark photon "effective width" $\Gamma_{A'}$ as a function of the A' mass for the case of the decay to scalar dark matter particles and for $\alpha_D = 0.1$ (red curve), compared with the energy resolution at the resonance peak of a "high-resolution" homogeneous calorimeter (blue curve) and a "low-resolution" detector (black curve). Right: CAD front view of the new high-resolution calorimeter.

vanishes as the center of mass energy of the e^+e^- pair moves away from the A' mass. For an experiment such as NA64, this behavior results in a clear signal signature, unique to this production channel: the missing-energy distribution features a peak, whose position depends on the A' mass. The peak results from the convolution of the resonant cross section with the positron track length in the active target, smeared by the intrinsic energy resolution of the ECAL. This feature can be exploited to improve the sensitivity of the experiment, e.g. by using ad-hoc "bump-hunt" analysis techniques. In this perspective, a good energy resolution of the active target is crucial to resolve correctly the missing energy peak. As an example, in the case of a vector A' decaying to scalar LDM, its width reads $\Gamma_{A'} \simeq \frac{m_{A'}}{12}\alpha_D$. In the laboratory frame a Jacobian factor $m_{A'}/(2m_e)$ appears, so that the effective A' width is $\Gamma^{eff}_{A'} \simeq \frac{m^2_{A'}}{24m_e}\alpha_D$. The energy resolution of a calorimeter as a function of the deposited energy E_{dep} can be parameterized as $\sigma(E_{dep}) = \alpha\sqrt{E_{dep}} \oplus \beta E_{dep}$; in the case of a resonantly produced A' $E_{dep} = E_0 - E_{A'} \simeq E_0 - m^2_{A'}/(2m_e)$, where E_0 is the initial beam energy and $E_{A'} = m^2_{A'}/(2m_e)$ is the energy of the produced A'. Therefore, the following requirement on the active-target energy resolution can be obtained:

$$\alpha\sqrt{E_{dep}} \oplus \beta E_{dep} < \frac{m^2_{A'}}{24m_e}\alpha_D \quad . \tag{3.3}$$

The black curve in Fig. 14, left panel, shows the energy resolution of a calorimeter with similar performance to the NA64 ECAL ($\alpha = 0.1\sqrt{GeV}$ and $\beta = 0.01$), as a function of the energy deposition corresponding to a resonantly produced dark photon of mass $m_{A'}$ (a 100 GeV positron beam was here considered); the red curve is the effective A' width in the lab frame, in the A' mass range of interest for the program proposed in this document.

From this result, we conclude that in the current setup, the energy resolution of the active target does not allow to properly resolve the A' peak in the missing-energy spectrum for $m_{A'} \lesssim 250$ MeV. In order to perform an optimized A' search in the 100 MeV - 200 MeV mass range, it is necessary to update the NA64 detector with a new high-resolution active target. In particular, we propose to replace the existing ECAL for the "Phase-II" measurement with the 40 GeV positron beam, since this beam configuration provides larger sensitivity to the lower $m_{A'}$ range.

The blue curve in Fig. 14 shows the resolution of a generic "high-resolution" calorimeter with $\alpha = 0.025\sqrt{GeV}$ and $\beta = 0.003$. Since a similar performance has been obtained by the CMS electromagnetic calorimeter [38], for the NA64 active target upgrade we focused on a homogeneous calorimeter of $PbWO_4$ crystals. The proposed detector consists of a 9x9 matrix of 20x20x220 mm^3 crystals, with four layers of crystals added in front, with the long axis oriented perpendicular to the beam direction, to act as a pre-shower. The total resulting length of the calorimeter is 34 X_0. The choice of the $PbWO_4$ material is motivated by its fast scintillating time ($\tau \simeq 10$ ns), well matched to the expected hit rate, its high density, allowing to construct a compact detector, and its high radiation hardness. The scintillation light is read out using SiPMs. A matrix of 4 photosensors, 6x6 mm^2 each, is optically coupled to one of the crystals' small faces. The performance of such a configuration was evaluated via Monte Carlo simulations. The detector was implemented within the official GEANT4-based simulation framework of the NA64 experiment, and a realistic modelization of the light readout chain, including energy-to-light conversion, photo-electron statistics, signal digitization and electrical noise was added. The missing energy resolution of the detector was thus evaluated by simulating sets of resonant A' production events for different $m_{A'}$ values.

The result are reported in Fig. 15, showing the measured energy distributions for fermionic (left) / scalar (right) LDM, considering different A' masses. We compare the results obtained including (continuous lines) or not (dashed lines) the digitization and readout effects. In the first case, the total energy is not corrected for the effect of the readout thresholds, hence the missing energy peak is slightly translated. From these results, we conclude that the PKR-CAL detector response does not affect significantly the A' line shape observed in the missing energy spectrum, even in the most stringent case of scalar LDM, where the A' width is smaller, confirming the validity of the present design.

R&D status The design and development of the new high resolution active target started in 2021 and it is currently in an advanced status. All the detector components ($PbWO_4$ crystals, SiPMs, electronics) have been tested and characterized. Dedicated light yield and radiation hardness measurements have been carried out for all the crystals composing the calorimeter, proving the compliance of the materials to the requirements defined in the design phase. The design of the mechanical structure of the detector is actually being finalized. Furthermore, a small-scale prototype of the detector was assembled and tested at the CERN H8 beamline, measuring the corresponding response to positrons and hadrons in the 10-100 GeV energy range, to assess the energy resolution and the linearity. Data analysis is currently in progress, but preliminary results (see Fig. 16) confirm the validity

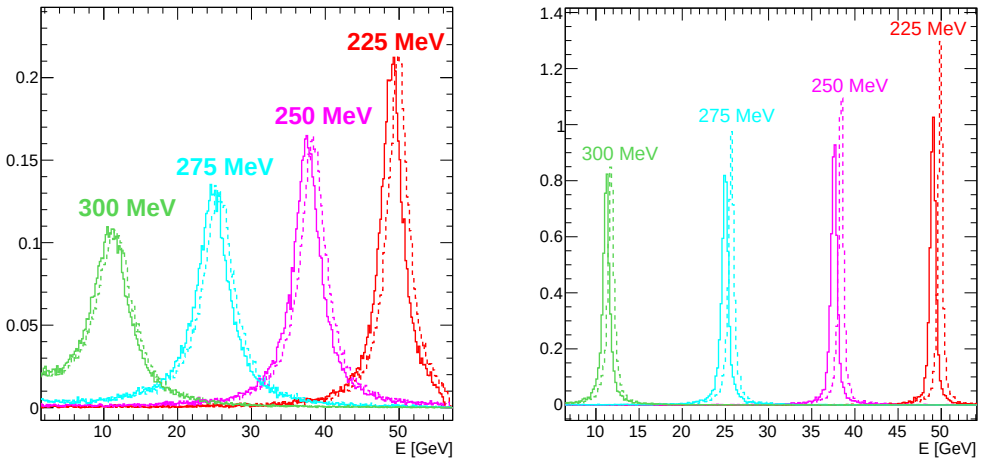

Figure 15. Left: the total energy measured by the PKR-CAL detector for missing energy events associated to A' resonant production, for different values of the dark photon mass, considering a vector A' decaying to fermionic LDM, with $\alpha_D = 0.1$. The continuous curves are the results obtained including all digitization and readout effects in the simulation, while the dashed curves represent the intrinsic detector response. The total energy is not corrected for the effect of the readout thresholds. Right: same as left, for scalar LDM.

of the detector design. A technical design report (TDR) of the detector is currently under preparation and will be made public before LS3.

3.3.3 The HCAL

The HCAL detector plays a crucial role in the NA64 search for invisibly decaying dark photons, since it allows to identify and reject events in which one or more energetic neutral hadrons are produced in the ECAL from electro- and photo-nuclear reactions by the impinging $e^{\pm}$ and exit from it, carrying away a significant fraction of the primary beam energy. Two possible types of background are associated to these event. In the first case (so-called "punch-through" scenario), leading neutral hadrons can pass undetected through the HCAL volume without any hard interaction. The probability for this effect, considering the overall length of the three HCAL modules downstream the ECAL of about $21\lambda_I$, can be estimated to be approximately 7.6×10^{-10}. Therefore, since only a fraction $\approx 10^{-5}$ of the impinging beam particles undergo an electro-/photo-nuclear reaction in the calorimeter, the expected background yield due to this effect is expected at the level of 10^{-14} per impinging particle. A detailed study of "punch-through" effects was actually performed in Refs. [39, 40], resulting to the same conclusion. A second contributing factor arises from resolution effects in the HCAL, leading to fluctuations in the measured deposited energy. Specifically, an event wherein one or more energetic neutral hadrons are generated in the ECAL and subsequently absorbed in the HCAL can mimic a signal if, due to these fluctuations, the measured E_{HCAL} value falls below the zero-energy threshold. This effect is discussed in more details in Sec. 4.4, and found to be actually the dominant background source for the proposed 40 GeV measurement.

The current HCAL design features a 3×3 matrix structure, comprising 47 layers in each cell. These layers consist of a 2.5-cm thick iron plate followed by a 4 mm thick plastic scintillator foil. Additionally, twelve 1-mm thick optical fibers, with attenuation length approximately 3 m, traverse longitudinally through every cell to collect scintillation light and transmit it to a PMT for readout – to avoid any possible energy leak, fibers are routed in a spiral. For this configuration, the nominal energy resolution is approximately$\sigma_{E_{HCAL}}/E_{HCAL} \simeq 70\%/\sqrt{E[\mathrm{GeV}]}$. In order to reduce the aforementioned effect, a dedicated R&D program is planned during CERN LS3 in order to improve the energy resolution, focusing on two distinct design upgrades.

First, we plan to study the effect of a longitudinal HCAL segmentation, with the detector divided into two equal halves with independent fibers readout, to suppress non-linear effects in the detector response induced by the optical fibers attenuation length. This effect is illustrated in Fig. 17, showing the deposited energy distributing in the HCAL precited from Monte Carlo for 100 GeV (left), 60 GeV (center), and 40 GeV (right) π^+, including (blue) or not (red) the optical fibers attenuation length in the simulation. We plan to test this solution already during the 2024-2025 period, adapting the current HCAL detector by splitting the optical fibers at the HCAL center and reading them out on both ends.

In parallel, we plan to study the possibility of a new HCAL design, with a denser

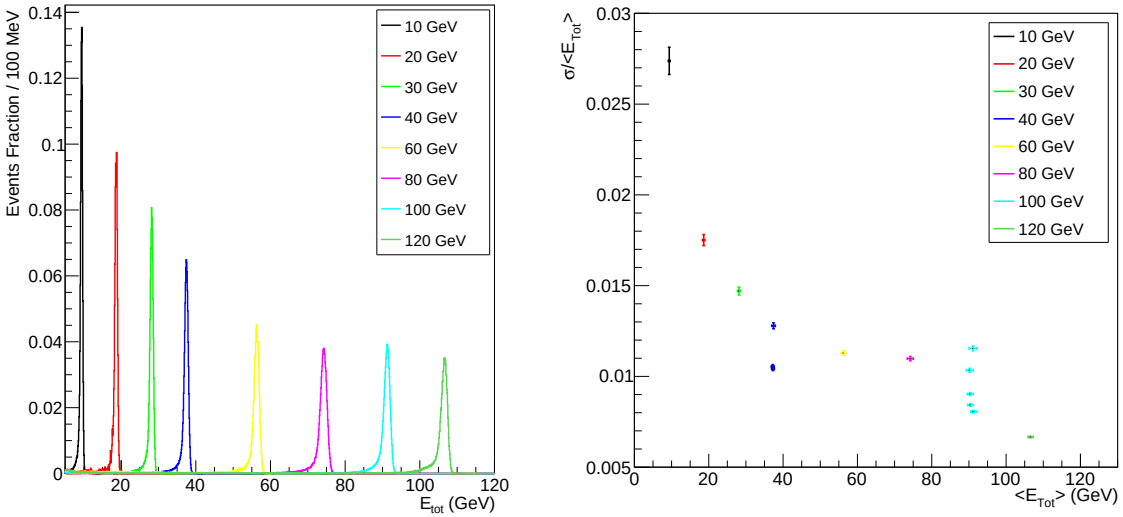

Figure 16. Left: the energy spectra measured by the prototype exploiting e^+ beams at different energies, as shown in the legend. Through these studies, we evaluated saturation effects in the detector response introduced by the finite number of pixels in the SiPMs. For the beam energies of our interest, we observed a response that slightly deviates from linearity and can be easily corrected to remove the saturation effects. Right: evaluation of the prototype's energy-measurement resolution as a function of the e^+ beam energy. Measurements with the 40 GeV and 100 GeV e^+ beam were repeated by closing the beam pipe collimators w.r.t. their nominal position. This resulted in a higher resolution estimate, showing that the energy dispersion of the beam limited our evaluation, which represents an upper limit of the actual prototype's resolution.

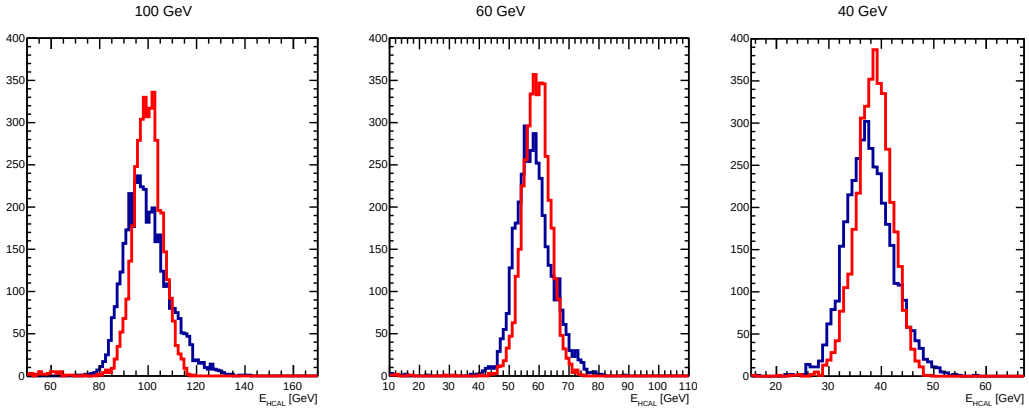

Figure 17. Simulated deposited energy distribution in the HCAL for 100 GeV (left) / 60 GeV (center) / 40 GeV (right) π^+, including (blue) or not (red) the optical fibers attenuation length in the simulation.

material for the absorbing layers. Some preliminary Monte Carlo studies were conducted in three configurations:

- The current configuration, mentioned above
- A configuration that includes 75 layers of lead, 1.6 cm thick (instead of iron)
- A configuration that includes 175 layers of tungsten, 0.4 cm thick (instead of iron).

For each configuration, $2{\cdot}10^4$ impinging pions π^+ were simulated, with energies equal to 100, 60, and 40 GeV, and the corresponding energy distribution in the HCAL was then fitted with Gaussian functions. The results are shown in Fig. 18. Thanks to these results, it is possible to obtain a trend of σ_E/E of the three HCAL configurations as a function of the beam energy: the results are shown in Fig. 19. As can be seen from the figure, the two new configurations improve the performance of the HCAL. This preliminary result suggests the possibility to improve the energy resolution by a factor $\simeq 2$ with the tungsten layers option.

Similarly to the SRD case, the specific upgraded HCAL detector design will be defined during LS3, based on the R&D measurements that will be performed during the next two years. All the background studies presented in this document were performed considering the current detector configuration.

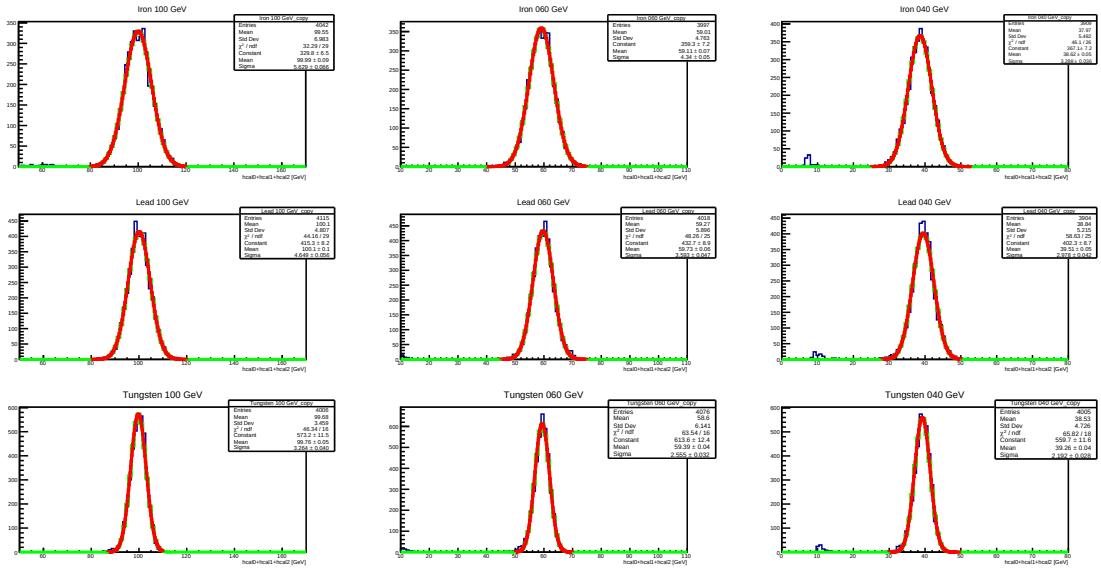

Figure 18. Results of the Monte Carlo studies on the different HCAL configurations. The first row shows the results obtained with the current configuration (iron) with a 100, 60, and 40 GeV π^+ beam (from the left to the right). The second row shows the results with the lead configuration, and, in the third row, with the tungsten. The red curves are the Gaussian function used to fit the distributions. The green curves are the prosecution of the red curves through all the range.

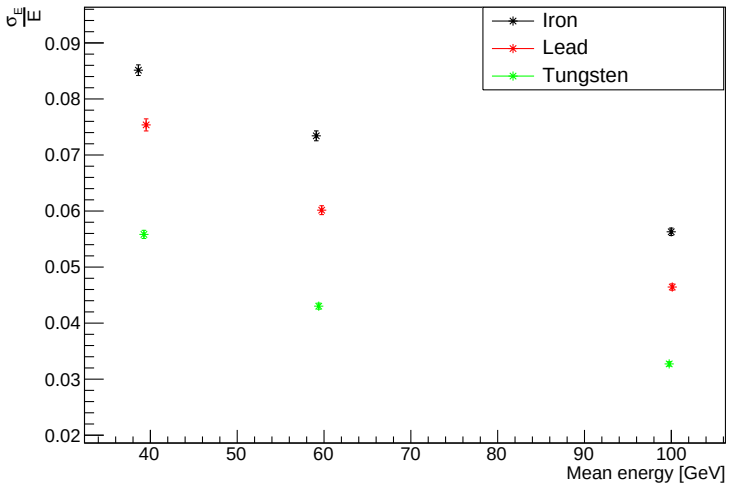

Figure 19. σ_E/E trends as a function of the beam energy for the different HCAL configurations.

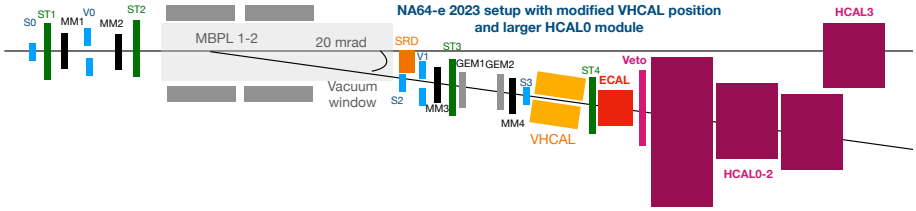

Figure 20. Same as Fig. 6, with modified VHCAL position and larger HCAL0 module.

4 Expected backgrounds

In this Section, we provide an estimate of the expected number of background events mimicking the signal signature, i.e. a well reconstructed upstream track in time with a SRD signal, paired with a missing energy in the ECAL of at least half of the beam energy and no activity in the VETO, HCAL, and VHCAL detectors.

The investigation of backgrounds at the level of a single event sensitivity for the accumulated statistics of $\simeq 10^{11}$ e^+OT via a full analytic Monte Carlo simulation would require a very large computing time. Furthermore, a "brute-force" strategy would entirely rely on the implementation within the simulation software of all background processes, with an accuracy level capable of predicting the yield of signal-mimicking rare-events at this level. Therefore, our estimates are based on a combination of MC simulations and positrons-beam measurements already performed at 100 GeV [1]. A summary of all expected background contributions is reported in Tab. 3, where the nominal values correspond to the results considering the nominal NA64$-e$ 2023 detector setup, while those in parenthesis refer to an optimized detector configuration, with the VHCAL position moved further downstream toward the ECAL (see Fig. 20) and with a slightly increased missing energy threshold.

From this estimate, we conclude that the proposed Phase-I and Phase-II measurements, performed with an optimized detector configuration, will be background-free, thus making the sensitivity directly proportional to the accumulated beam charge. A dedicated R&D program will be completed before LS3 to support these numbers and to demonstrate the Monte Carlo simulation results regarding the new detector configuration.

4.1 Upstream interactions

The hadron production from the interaction of the primary positron beam with the upstream materials of the beamline, occurring either directly or via the emission of a real Bremsstrahlung photon, may give rise to a background event, if the produced hadrons falls out of the acceptance of the detector, while the soft final state e^+, emitted at large angle, is still transported by the dipole magnet toward the ECAL. This would result in a small ECAL energy deposition and no activity in the HCAL. The energy dependence of the cross section for electro- and photo-nuclear processes in the multi-GeV regime implies that the normalized yield of these background events is similar to the result already observed at 100 GeV positron beam energy [37]. However, in the low-energy kinematic regime particles

are typically emitted at larger angle, thus making this background source potentially more relevant. The use of the VHCAL detector will thus be crucial to suppress it.

In order to evaluate the corresponding yield, we performed a dedicated FLUKA simulation for each positron beam energy, introducing an artificial bias factor $\times 1000$ for the cross section of electro- and photo-nuclear reactions[5]. For both beam energies, accounting for the biasing factor, an equivalent number of 5×10^{10} e^+OT was simulated; this corresponds to half of the proposed statistics for the positron program.

For this study, we considered at first the 2023 NA64$-e$ detector configuration. We applied the following selection cuts to the Monte Carlo events: the deposited energy in the HCAL3 must be less than 1 GeV, the deposited energy in each VETO panel must be less than 8 MeV, and finally the deposited energy in the VHCAL must be less than 800 MeV. We also required that the impinging positron track is properly reconstructed within a 5-σ momentum window centered around the nominal value; the track quality is imposed with a 1% p-value cut. We verified that the corresponding efficiency for full-energy positrons not undergoing any hard interaction before hitting the ECAL is higher than 80% both at 40 GeV and at 60 GeV.

The results for the 60 GeV simulation are shown in Fig. 21, top row, reporting the HCAL-vs-ECAL energy distribution for all selected events (top-left plot): an accumulation of events with $E_{ECAL} < E_0$ and $E_{HCAL} \simeq 0$ is observed. We investigated these events and we confirmed that they are all associated with the production of upstream hadrons outside the HCAL acceptance, as expected. Therefore, to evaluate the expected background yield, we adopted a strategy similar to that used for the 100 GeV e^+ beam data analysis, extrapolating from the bulk of the E_{ECAL} distribution to the signal region with an exponential function, as shown in the top-left plot of Fig. 21. The obtained background prediction is

[5]Biasing was activated only for the detector volumes located upstream the ECAL.

Background source	Background (60 GeV)	Background (40 GeV)
(i) e^+ hadronic interactions in the beam line	0.03 (1.4×10^{-4})	2.7 (0.04)
(ii) Hadron decays (K/π)	$0.009 + 0.04$	$0.002 + 0.02$
(iii) μ decays	6×10^{-3}	9×10^{-4}
(iv) e^+ hadronic interactions in the target	$\sim 10^{-3}$	$\sim 10^{-3}$
(v) HCAL energy resolution effects	$1.70{\cdot}10^{-2}$	1.59 (0.09)
(vi) di-muons	≤ 0.0021	≤ 0.0015
Total n_b (conservatively)	~ 0.2	~ 4.4 (0.2)

Table 3. Expected background yield for 10^{11} accumulated e^+OT for the two positron beam measurements at 60 GeV and 40 GeV. For the first background source listed in the table, the reported yield refers to the nominal NA64$-e$ 2023 detector configuration, while the number in parenthesis is the result obtained considering an optimized setup with the VHCAL moved further downstream toward the ECAL. For the fifth background contribution, instead, the number in parenthesis for the 40-GeV measurement correspond to a slightly increased missing energy threshold. See text for further details.

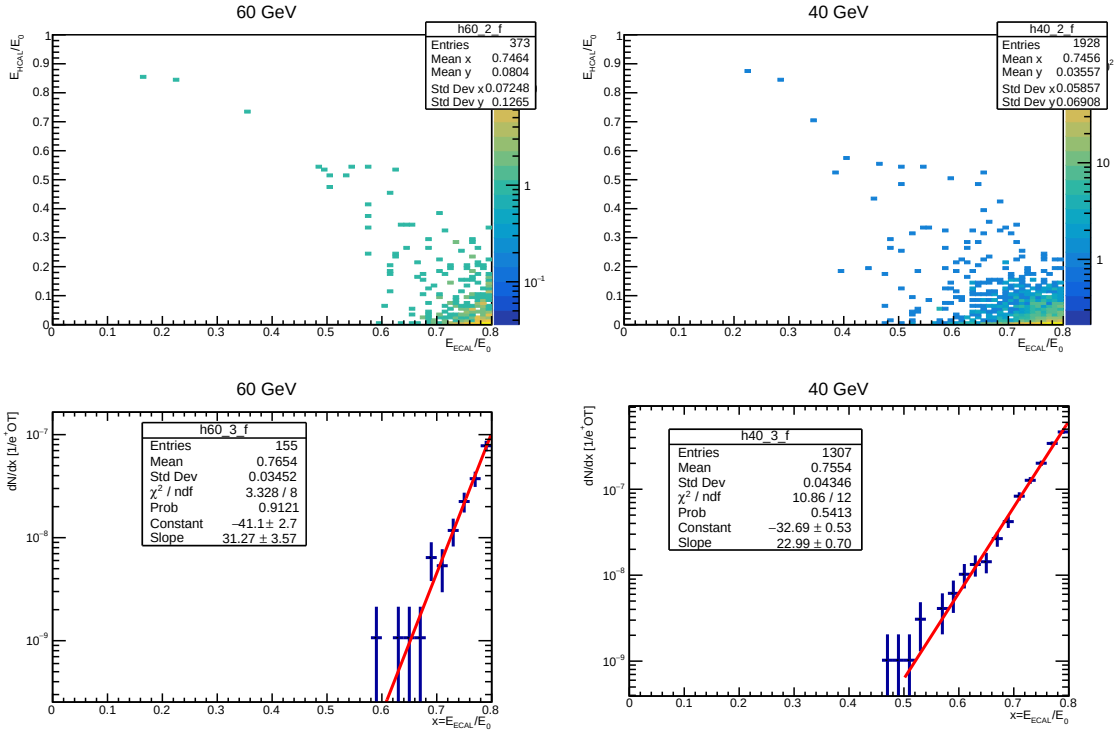

Figure 21. Results from the analysis of Monte Carlo simulations for the study of backgrounds induced by upstream electro- and photo-production of energetic hadrons, at 60 GeV beam energy (left column) and 40 GeV beam energy (right column). Top-left: the ECAL vs HCAL energy distribution for selected events considering the NA64−e 2023 detector setup. Bottom-left: the ECAL energy distribution for events selected after a 1 GeV cut on the total HCAL energy, normalized to the total number of simulated events. All energies are scaled to the primary beam energy. Top-right and bottom-right: same as top, for the 40 GeV beam energy simulation.

$\simeq 0.03$ events for the full statistics of 10^{11} e^+OT.

The same result for the 40 GeV beam energy is shown in Fig. 22, bottom row. In this case, a larger number of events with $E_{ECAL} < E_0$ and $E_{HCAL} \simeq 0$ is observed, again due to the production of upstream hadrons outside the HCAL acceptance. The same extrapolation procedure adopted for the 40-GeV simulation predicted a total number of $\simeq$ 2.7 background events for the full statistics of 10^{11} e^+OT within the signal window.

In order to identify a strategy to reduce this background contribution, we further scrutinized the events close to the signal window. We concluded that their majority originates from electro-nuclear interactions occurring in the detector elements installed just upstream the ECAL, namely the last MicroMega detector and the last plastic scintillator trigger counter, with the final state hadrons emitted at large angle, outside the HCAL acceptance. Therefore, we considered an alternative detector configuration in which the position of the VHCAL is moved further downstream toward the ECAL, with the aforementioned detectors installed before it (see also Fig. 20). In addition, we considered to replace the first HCAL detector (HCAL0) with the one having larger transverse dimensions (120×60 cm^2) already developed for the NA64-μ program. The results are shown

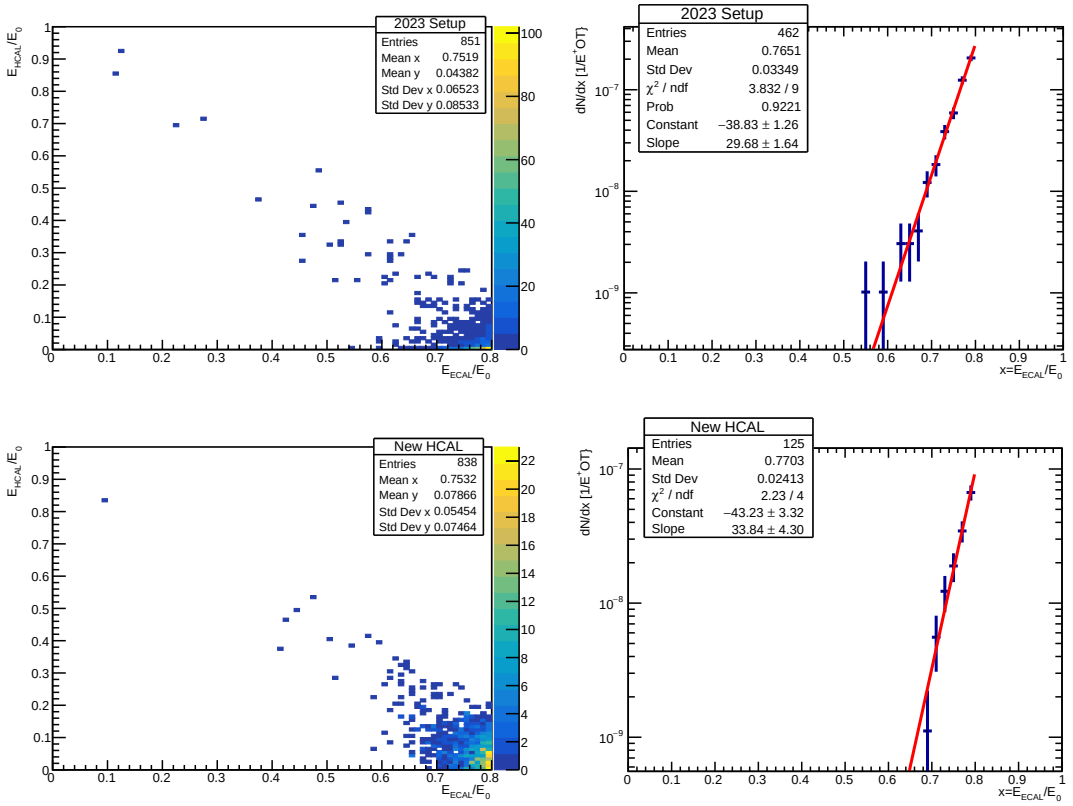

Figure 22. Same as in Fig. 21, for the new detector configuration with the VHCAL moved further downstream toward the ECAL.

in Fig. 22. We observe that, for both beam energies, the background yield is drastically reduced, with a predicted value of 1.4×10^{-4} (0.04) for the 60 GeV (40 GeV) measurement.

These studies underline the critical role of the VHCAL detector in suppressing backgrounds due to upstream beam interactions with beamline materials. We underline that the current 2023 VHCAL detector, whose design was here considered, is a first prototype, and further R&D work is planned in NA64 to construct the final detector version.

4.2 Hadrons and muons in-flight decay

The in-flight decay of an impinging hadron or muon to a final state involving a soft electron and an energetic neutrino can mimic the signal signature. In principle, this background is highly suppressed by the SRD cut. Nevertheless, there may still be cases in which a δ electron is knocked out by the hadron/muon in the upstream beamline elements (in particular, the downstream vacuum window), and hits the SRD giving rise to a signal similar to the one expected from e^+ synchrotron radiation. Similarly, the random superposition of a hadron/muon and a low-energy positron from the beam tail within the typical response time of the detector ($\simeq 30 \div 40$ ns) can give rise to a background event, if the e^+ emits enough synchrotron radiation to satisfy the SRD cut and is then deflected away

by the bending magnet, and the hadron decays in flight. The magnitude of these effects can be evaluated directly from data. The δ-ray emission probability can be measured exploiting data collected in "open-trigger" mode, without the lead conversion target[6], while the intensity of the low-momentum tail of the beam can be estimated from a calorimetric measurement, acquiring data with zero magnetic field and with the ECAL placed on-axis at zero degree [1]. Here, we conservatively assumed a δ-ray emission probability of about 10^{-2} per impinging muon/hadron, extrapolating the result from the measurement performed with a 100 GeV positron beam to a SRD threshold of $\simeq$ 500 keV, and considering the current detector configuration. We neglected the contribution of the second effect (low-energy beam tail), since, as suggested from the 100 GeV e^+ measurement, its magnitude is significantly suppressed with respect to the $\delta-$ray emission[7].

The most critical decay channels are the $K^+ \to e^+\pi^0\nu$ reaction (K_{e3} decay), when the neutrino carries away a large fraction of the beam energy and the positron and the two photons from π^0 decay are collimated forward and give rise to a single, low energy EM shower in the ECAL, the branching-ratio suppressed $\pi^+ \to e^+\nu_e$ decay, and finally the $\mu^+ \to e^+\overline{\nu}_\mu\nu_e$ decay. To evaluate the corresponding yields, we performed dedicated FLUKA simulations of the NA64 setup for an impinging $K^+/\pi^+/\mu^+$, considering for simplicity the existing ECAL detector, and introducing ad-hoc biasing factors to each particle mean life to enhance the statistical sample. In each simulation, we computed the fraction of particles decaying within the NA64 acceptance, with a signal-like signature, assuming a 50% missing-energy threshold and a 1 GeV threshold for the HCAL. Specifically, we applied a 800 MeV cut to the total energy deposited in the VHCAL, and required the presence of a well-reconstructed track ($p_{val} > 0.01$) within a $\pm 5\sigma$ window centered at the nominal momentum value. To compute the absolute background yields, the following normalization factors were adopted. The beam hadronic contamination at 60 GeV (40 GeV) was computed from a dedicated Monte Carlo simulation, validated with data at 100 GeV, and found to be $\eta_h = 0.3\%$ ($\eta_h = 0.03\%$). The fraction of pions f_π at the converter was found to be $\simeq 10\%$. However, as discussed in Ref. [27], this number does not account for the fact that, due to mass-dependent effects such as synchrotron radiation emission, protons are transported by the H4 beamline with lower efficiency than π^+, thus increasing the measured value of f_π at the NA64 detector location. We thus decided to estimate f_π from the experimental result from Ref. [27], scaling it for the increased ratio at the converter, obtaining $f_\pi \simeq 60\%$. The π/K ratio was fixed to the value measured from the 100 GeV positron data-set, $\pi/K \simeq 400$. The muon contamination η_μ was also estimated from the 100 GeV result, starting from the measured μ/π ratio ($\mu/\pi \simeq 0.1\%$) and introducing an appropriate scaling factor to account for the reduced hadrons lifetime, and hence for the larger number of parent pions/kaons decaying in the H4 beamline. Finally, a typical signal efficiency of 50% was assumed, in line with the result from the 100 GeV measurement.

[6]The "open-trigger" mode requires solely the coincidence between the signals from the plastic-scintillator based beam-defining counters to initiate detector readout.

[7]We also expect that, operating with a lower beam energy, given the higher e^+ intensity from the conversion target, it will be possible to further close the momentum-collimating slits to almost completely suppress the low-energy tails.

The obtained results, summarized in Tab. 3, predict a total background yield from hadrons decay of about 0.05 events (0.022 events) at 60 (40) GeV beam energy; in both cases, the contribution from muons decay is suppressed by more than one order of magnitude.

4.3 ECAL and HCAL punch-through

Events with one or more high-energy hadrons electro-/photo-produced in the ECAL and passing undetected through the VETO and the HCAL can mimic the signal signature. The production of hadrons can be either due directly to an electron/positron, $eZ \to eZX + h$, or a Bremsstrahlung photon of the shower developing in the target, $\gamma Z \to Xh$. In both cases, the most critical source of background events is that due to the production of a single, energetic long-lived neutral hadron (neutron, K_L) passing undetected through the VETO and not releasing any energy within the HCAL.

For the measurement performed with a positron beam at 100 GeV, this background contribution was estimated with a data-driven approach, evaluating the HCAL punch-through probability for hadrons from the data collected in "open-trigger" mode. This was found to be $f_{punch-through} \simeq 0.4\%$ [27], for each HCAL module. Here, we assume the same result for the two measurements at 60 GeV and 40 GeV, given the modest dependency of the hadron interaction cross section on the impinging particle energy in this energy range. Similarly, we scaled the number of expected electro-nuclear events in the ECAL from the 100 GeV dataset, where a yield of about 2200 events with $E_{ECAL} < E_0/2$ was observed for a total statistics of approximately 10^{10} e^+OT. Scaling this number to the expected statistics of 10^{11} e^+OT, the final number of expected background events for each measurement is:

$$B_{enh}^{punch-through} \simeq N_{enh} \cdot (f_{punch-through})^3 \simeq 1 \times 10^{-3} \quad , \tag{4.1}$$

where $N_{enh} \sim 2 \times 10^4$ is the expected number of electro-production events in the ECAL.

4.4 HCAL energy resolution effects

A second potential background source related to electro/photoproduction reactions occurring in the ECAL, for events in which the full beam energy is deposited in both the ECAL and the HCAL, arises from fluctuations in the HCAL response. These fluctuations could lead to the reconstruction of an event within the signal box (SB) $E_{ECAL} < E_0/2$, $E_{HCAL} \lesssim 1$ GeV. To estimate this background yield, we exploited data collected in the 100-GeV e^+ run, corresponding to a statistic of 10.8×10^9 e^+OT; the results obtained for the 100 GeV run have then been extrapolated for the 40 GeV and 60 GeV measurements, adopting the procedure described in the following.

Background estimation from the 2022 100 GeV positron run We isolated events in which an electro/photoproduction interaction occurred in the ECAL, and we considered the corresponding HCAL distribution in the SB. These events lay in the diagonal portion of the E_{HCAL} VS E_{ECAL} "hermeticity" plot, as reported in Fig. 4, left panel. The cuts used for this analysis are the same as those described in Sec. 2. The extrapolation was performed by dividing data in different sub-sets, based on the ECAL energy (from 0 GeV

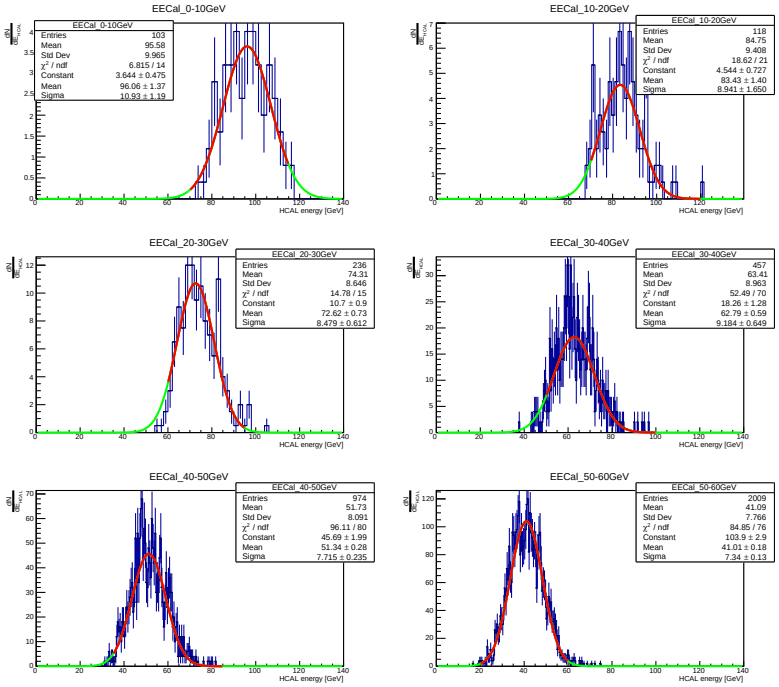

Figure 23. HCAL energy distribution for every ECAL data sample. The red curves are the Gaussian function used to fit the distributions. The green curves are the prosecution of the red curves through all the range.

to 60 GeV in 10 GeV steps). For each of these intervals, the corresponding HCAL energy distribution was fitted with a Gaussian curve, as shown in Fig. 23. For each interval, the background yield due to low-energy HCAL fluctuations was thus obtained by integrating the corresponding energy distribution in the SB interval:

$$N^i_{SB} = \int_0^{1\,\mathrm{GeV}} g^i(E)dE \ , \tag{4.2}$$

where $g^i(E)$ is the Gaussian function that parameterizes the HCAL energy distribution for the $i-$th interval. The total number of events in the SB is then obtained by summing up all N^i_{SB} contributions. For this study, only the data samples with ECAL energy deposition up to 50 GeV were considered. We underline that this is a conservative estimation since we are assuming that the response of all HCAL cells simultaneously fluctuates towards the SB. To verify the effect of the uncorrelated contributions of the detector response, we repeated the procedure after imposing a 1 GeV upper limit on the energy deposited in the second HCAL module E_{HCAL-1}. The result reads 0 background events, also when the 1 GeV cut is applied: this is due to the marked separation between the hermeticity plot diagonal and the SB.

Background evaluation for the 40 GeV and 60 GeV proposed measurements To extrapolate the number of events expected in the SB for a 60 (40) GeV beam, we built two ad-hoc data sets, starting from the sample used for the 100 GeV study described in

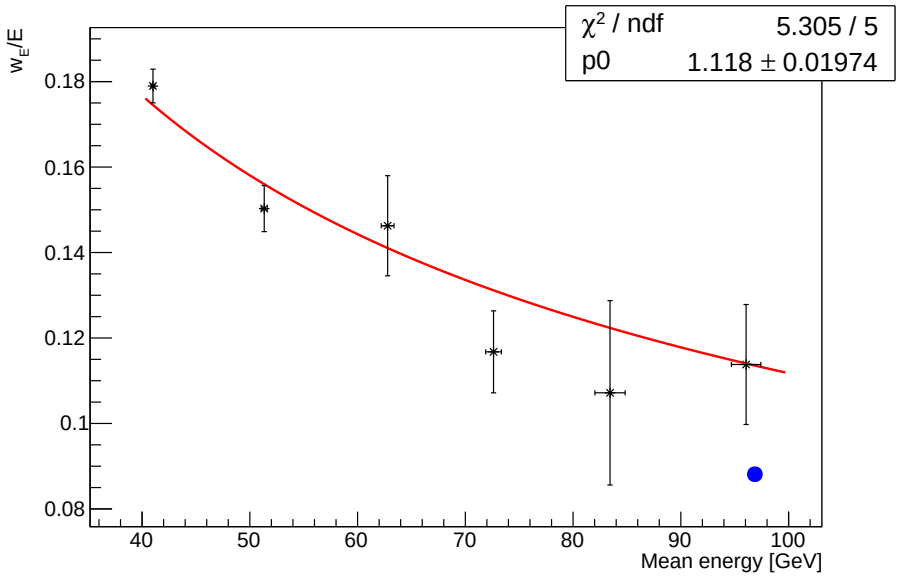

Figure 24. Trend of the HCAL w_E/E as a function of the mean energy, obtained from the analysis of electro/photoproduction data subsets. The blue dot corresponds to the HCAL resolution σ_E/E result obtained from a direct 100 GeV measurement, performed exploiting the hadronic contaminants in the beam - mostly protons -, by selecting events with a MIP-like signature in the ECAL and VETO, and then measuring the corresponding HCAL energy distribution. As expected, the measured w_E/E for a deposited energy equal to 100 GeV is larger than the σ_E/E. The red line is the result of the best fit performed with the function $f(x)$.

the previous paragraph. To build the new data sets, we re-scaled the ECAL energy of the data collected at 100 GeV to the beam energies of the proposed measurements (60 GeV and 40 GeV). The two data sets were then divided into five ECAL energy intervals from 0 to half the beam energy. For each interval, we considered a hypothetical HCAL energy distribution, whose shape was obtained by extrapolation from the 100 GeV dataset. Specifically, from the fits to the 100-GeV beam energy HCAL intervals presented in Fig. 23, we measured the parameter w_E, which is the convolution of the resolution of the HCAL, the resolution of the ECAL, and the width of the considered ECAL energy bin. These w_E parameters are the σ parameters of the Gaussian fits shown in Fig. 24, and the trend w_E/E as a function of the energy was then fitted with the function $f(x) = \frac{p_0}{\sqrt{E}}$. As a reference, the blue marker in the figure corresponds to the value of σ_E/E derived from a calibration run carried out with 100 GeV secondary protons[8], selecting the events that deposit their entire energy in the HCAL. This value is in line with the results from Fig. 23, confirming

[8]When the H4 beamline is operated in positive-charge mode, the yield of secondary hadrons is mostly due to protons from the $\Lambda \to p\pi^-$ decay chain. For further details, see e.g. Ref. [27].

a trend of w_E/E as follows [9]:

$$\frac{w_E}{E} \simeq \frac{1.1}{\sqrt{E\,[\mathrm{GeV}]}} \tag{4.3}$$

The expected background yield at 60 (40) GeV beam energy was then obtained by integrating, for each hypothetical dataset, the corresponding HCAL distribution within the SB, and then summing up all contributions. As before, we accounted for uncorrelated effects in the HCAL response by introducing a 1.7 (2.5) GeV upper cut on E_{HCAL-1}. This value was raised with respect to the 100 GeV analysis to account for the lower beam energy.

The final results are reported in Tab. 4. The current HCAL design results in a negligible number of background events for a 60 GeV e^+ measurement with 10^{11} e^+OT, while the yield for a 40 GeV run with the same statistics is sizable, although all events come from the last ECAL slice. This is to be considered an indicative and preliminary result, that shows, however, how crucial the HCAL energy response is for the low-energy positron-beam program. During the pre-LS3 R&D program, we plan to carry out more in-depth calibration studies, using new custom equipment currently under development. This includes a mechanical platform that allows to change the position of each HCAL module and align each cell with the primary beam, to measure the corresponding full-energy response and thus obtain a more precise calibration constant. Furthermore, to reduce this background, during LS3 we plan to study how to further optimize the resolution of the HCAL, by improving the current detector design as discussed in Sec. 3.3.3.

4.5 Di-muons background

Another possible background may arise from di-muon events, i.e. events where an energetic pair of muons is produced in the ECAL from the annihilation of a positron or the conversion of a secondary photon from the electromagnetic shower. Usually, these events are rejected using the VETO and the HCAL, where each muon deposits an average energy of 2 GeV per HCAL module, due to ionization. However, events can produce a background if both muons are not detected by the VETO, due to detector inefficiency, and their reconstructed HCAL energy is lower than 1 GeV, due to HCAL resolution effects. A rough estimate of

[9] For the NA64 2022 run, the calibration of the HCAL modules was performed with a muon beam, due to unavailability of the dedicated calibration platform, resulting in a worse energy resolution than what was expected. The results shown in Fig. 24 and Eq. 4.3 are to be considered a conservative estimate.

ECAL Slice [GeV]:	Events in Signal Box:	ECAL Slice [GeV]:	Events in Signal Box:
0-6	0	0-4	$3.00{\cdot}10^{-5}$
6-12	0	4-8	$4.43{\cdot}10^{-4}$
12-18	$5.00{\cdot}10^{-6}$	8-12	$5.32{\cdot}10^{-3}$
18-24	$1.95{\cdot}10^{-4}$	12-16	$7.92{\cdot}10^{-2}$
24-30	$1.68{\cdot}10^{-2}$	16-20	1.50
Total events in SB:	$1.70{\cdot}10^{-2}$	Total events in SB:	1.59

Table 4. Number of events in the signal box in each ECAL energy bin for a beam energy equal to 60 (40) GeV on the left (right). All results reported in this table are already scaled considering a statistic of 10^{11} e^+OT.

such background for the measurements proposed in this document was performed starting from the analysis of 2022 100 GeV positron data (See Sec. 2 for a summary of the 100 GeV positron data analysis). The procedure adopted consists of two steps: first, the expected di-muon background for the 100 GeV positron beam measurement is evaluated from data; then, the obtained result is extrapolated for the 60 GeV and 40 GeV beam energy measurement, exploiting two ad-hoc factors calculated via Monte Carlo simulations.

Di-muons background estimation from the 2022 100 GeV positron run As previously mentioned, such background arises from events where muon pairs produced in the ECAL are not correctly detected by both the VETO and the HCAL; the detection inefficiencies of these two detectors were evaluated separately. As a first step, we evaluated the di-muon tagging efficiency of the VETO. Di-muon events were selected using all the cutflow described in 2, excluding the ECAL and HCAL cuts. To identify di-muons, the following HCAL selection cuts were added:

- (HC2 $>$ 2 GeV) or (HC011 $>$ 1.5 GeV and HC111 $>$ 1.5 GeV and HC2 $>$ 1.3 GeV), where HC2 is the third HCAL module, HC011 is the central cell of the first HCAL module and HC111 is the central cell of the second HCAL module.
- For each HCAL module, the energy deposition had to be in the range (4-8) GeV

These cuts, optimized to select two MIPs crossing the HCAL, led to a clean di-muon sample selection; then, the VETO cut was applied (for each VETO module the deposited energy had to be lower than 13.5 MeV[10]): the di-muon rejection inefficiency resulted equal to (0.23$\pm$0.02)%.

After the evaluation of the di-muon rejection inefficiency of the VETO, we proceeded to estimate from data the expected number of di-muon events with energy deposition in the ECAL in the 0 GeV - 50 GeV range that are reconstructed with HCAL energy lower than 1 GeV, due to the finite energy resolution of this detector. Such is in fact the definition of the signal window for the 2022 100 GeV positron data. For this study, we selected all the di-muon events in the positron production runs (corresponding to a total of $\sim 10^{10}$ e^+ on target), by applying to data the complete cutflow, excluding cuts involving the VETO and the HCAL.

We then selected events with total HCAL energy lower than 25 GeV, and ECAL energy within the range of 0 GeV - 50 GeV. This selection results in a clear di-muon sample (total of $\sim 2.3 \times 10^5$ events), as shown in Fig. 25, right panel. In order to estimate the probability for a di-muon event to be reconstructed with HCAL energy within the signal region ($E_{HCAL} < 1$ GeV), we adopted the following procedure. The selected sample was divided into five subsets, based on the ECAL energy (from 0 GeV to 50 GeV in 10 GeV steps). This separation was made to check for any differences depending on the di-muon pair energy. The differential events distribution as a function of the HCAL energy $\frac{dN_i}{dE_{HCAL}}$

[10]The cut value chosen is consistent with the NA64 2022 electron analysis. We emphasize that, during the analysis of the proposed positron measurements, the veto cut value will be further optimized to maximize the experiment sensitivity. We also stress that, given the lower beam energy, the veto efficiency for signal events would be higher for a fixed threshold value.

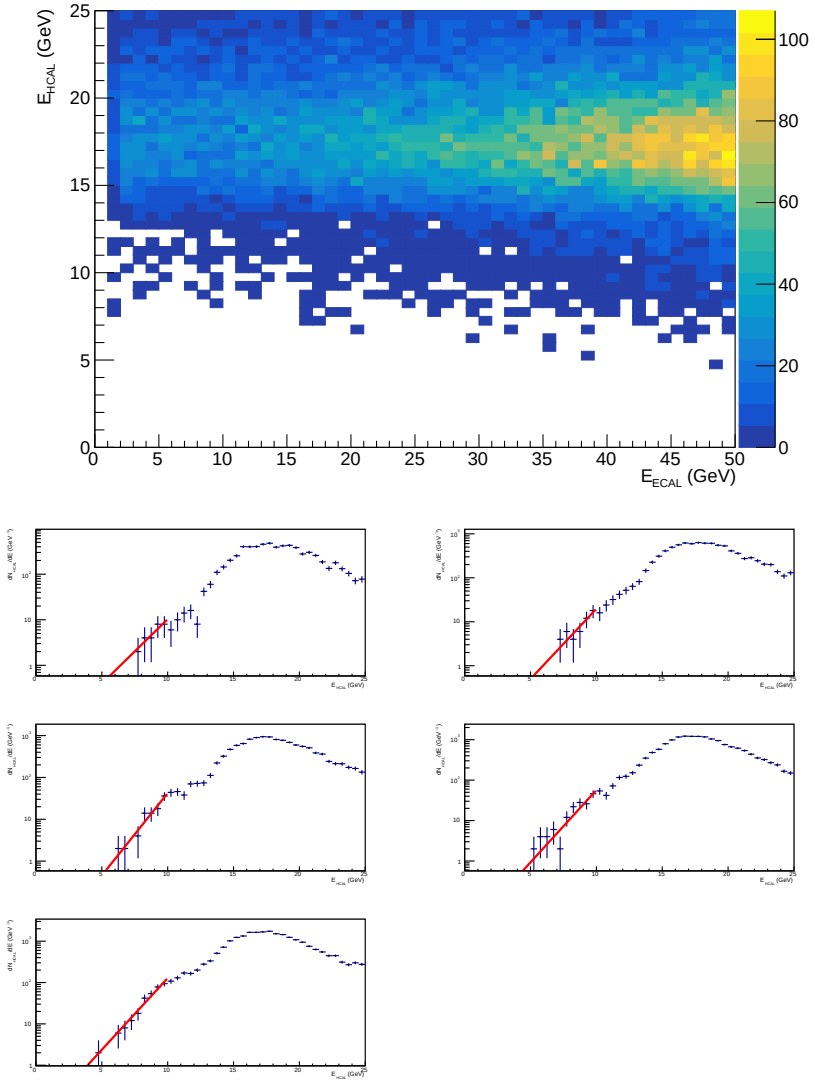

Figure 25. Upper panel) E_{HCAL} VS E_{ECAL} 2D histogram of the di-muon sample obtained by applying the cuts described in the text to the whole 100-GeV positron data. Lower panel) The plots show the differential di-muon event distributions corresponding to different ECAL energy bins, with the exponential curves used to fit the low-energy range (red curves).

was built for each i-th subset; the low energy part of the spectra was then fitted with an exponential function. Figure 25, right panel, shows all the fitted $\frac{dN_i}{dE_{HCAL}}$. The exponential curve was chosen as fit function since such a functional form describes with reasonable accuracy the low-HCAL-energy tails of the di-muon sample. It is worth noticing that the distributions of the different subsets present similar shapes, which is consistent with the weak dependence of the energy deposition in the HCAL from the kinetic energy of the muons, behaving as MIPs. To get the number of expected background events, the fitted functions were used as parametrizations of the $\frac{dN_i}{dE_{HCAL}}$ and finally integrated in the 0 GeV - 1 GeV HCAL signal range. The five obtained values were summed, so to get the expected

number of events in the signal box $N_{SB}^{2\mu}$:

$$N_{SB}^{2\mu} = \sum_{N=1}^{5} \int_{0}^{1\text{GeV}} \frac{dN_i}{dE_{HCAL}} dE_{HCAL} \tag{4.4}$$

In order to evaluate the systematic error associated with this procedure, we calculated $N_{SB}^{2\mu}$ varying the upper limit of the energy interval for the exponential fit, in the range 10 GeV - 15 GeV. The obtained values varied significantly depending on the fit range: to obtain a conservative background estimate, we decided to consider the maximum value $N_{SB\ max}^{2\mu} \simeq 1.2$ events. This quantity represents an upper limit for the expected number of di-muon events reconstructed by the HCAL with an energy $E_{HCAL} < 1$ GeV, before the application of the VETO cut. Therefore, as a final step, the di-muon expected background $N_{BKG\,100\,GeV}^{2\mu}$ can be obtained by multiplying $N_{SB\ max}^{2\mu}$ by the VETO detection inefficiency for di-muons, whose evaluation procedure was previously described:

$$N_{BKG\,100\,GeV}^{2\mu} \leq N_{SB\ max}^{2\mu} \times 0.0023 \simeq 0.0028. \tag{4.5}$$

Di-muons background evaluation for the 40 GeV and 60 GeV proposed measurements The di-muons background estimates for the 40 GeV and 60 GeV positron runs proposed in this document were carried out by extrapolating the result obtained from the 100 GeV positron data $N_{BKG\,100\,GeV}^{2\mu}$. The robustness of this procedure, here described, is motivated by the fact that, in first approximation, muons behave as MIPs in a large energy range. Therefore, their energy deposition in the VETO and HCAL is not strongly affected by their initial kinetic energy; this assumption is corroborated by Fig. 25, right panel. Indeed, even for the 40 GeV beam measurement, we plan to apply a missing energy threshold on the ECAL of ~ 20 GeV; as a result, the total kinetic energy of di-muon pairs that can produce background has to be larger than ~ 20 GeV. In conclusion, since muons with kinetic energies larger than ~ 1 GeV behave as MIPs, we assume that the HCAL energy spectrum for di-muon events produced in the 100 GeV positron run is representative of the di-muon spectra of the proposed 40 GeV and 60 GeV runs. In light of this assumption, the expected di-muons background contributions for the proposed measurements $N_{BKG\,40,60\,GeV}^{2\mu}$ can be roughly evaluated as follows:

$$N_{BKG\,40,60\,GeV}^{2\mu} \simeq \frac{N_{e^+OT\ 40,60\,GeV}}{N_{e^+OT\ 100\,GeV}} \cdot N_{BKG\,100\,GeV}^{2\mu} \cdot f_{40,60\,GeV}.$$

Here, $N_{e^+OT\ 40,60\,GeV} = 10^{11}$ is the expected statistics for the proposed low-energy measurements, $N_{e^+OT\ 100\,GeV} = (10.1 \pm 0.1) \times 10^9$ is the total statistics collected during the 2022 positron run and $f_{40,60\,GeV} = 0.53, 0.79$ are two normalization factors obtained from MC, accounting for the different di-muon production yields at 40 GeV and 60 GeV with respect to the 100 GeV measurement. These $f_{40\,GeV}$ and $f_{60\,GeV}$ factors are obtained as follows. Three different Monte Carlo simulations of the positron beam impinging on the NA64$-e$ detector have been performed, at 40 GeV, 60 GeV, and 100 GeV beam energy. These simulations, performed using the NA64 Monte Carlo framework, were used to estimate the number $N_{100,60,40\,GeV}^{2\mu}$ of di-muon events produced per positron on target in the

ECAL, for the different beam energies. The simulated samples were analyzed by imposing a rough di-muon selection cut, asking for a double-MIP energy deposition (between 1.5 GeV and 8 GeV) in at least one of the HCAL modules. In addition, a cut was applied on the ECAL energy, requiring that $(E_{ECAL} - E_{beam}) < E_{beam}/2$. This last selection was used to identify those di-muon events that may result in a large missing energy and therefore in a background. The numbers of events surviving these cuts, for each beam energy simulated, were used to define $f_{40\,GeV}$ and $f_{60\,GeV}$:

$$f_{40\,GeV} = \frac{N^{2\mu}_{40\,GeV}}{N^{2\mu}_{100\,GeV}} \simeq 0.53 \quad ; \quad f_{60\,GeV} = \frac{N^{2\mu}_{60\,GeV}}{N^{2\mu}_{100\,GeV}} \simeq 0.79$$

Given the definition of the factors $f_{40,60\,GeV}$, this procedure is not strongly affected by systematic errors introduced by the Monte Carlo simulations. In conclusion, the expected di-muon background for the two proposed measurements are:

$$N^{2\mu}_{BKG\,40\,GeV} \leq 0.015 \quad ; \quad N^{2\mu}_{BKG\,60\,GeV} \leq 0.021.$$

These results represent a first indication of the contribution of this source to the total background yield; the data collected during the preliminary measurement campaign proposed in 2024 and 2025 (see next Sections) will be used to further improve and validate this study.

5 Expected sensitivity

The expected sensitivity for the proposed measurement, as a function of $m_{A'}$ is shown in Fig. 26, for fermionic LDM, with $\alpha_D = 0.1$ and $m_{A'} = 3m_\chi$, compared with the most updated upper limits from NA64 [1, 21] and BaBar [22]. The NA64 result includes both the limit from the $\simeq 10^{12}$ electrons-on-target measurement at 100 GeV and that from the $\simeq 10^{10}$ positrons-on-target one at the same energy. As discussed before, for both positron measurements a total accumulated statistics corresponding to 10^{11} e^+OT was considered, assuming a missing energy threshold corresponding to half of the beam energy and a 50% signal efficiency, in analogy with the analysis strategy adopted for the 100 GeV data analysis. We underline that, during operations, we will set the missing-energy trigger threshold to the smallest value compatible with DAQ operations (max readout speed $\simeq 30$ kHz), thus leaving room for further optimization during the subsequent offline analysis.

Based on the estimate discussed in Sec. 4, we evaluated the sensitivity in the hypothesis of no background events within the signal window, adopting for the latter a conservative missing-energy cut equal to half of the primary beam energy. In the figure, the cyan (green) curve shows the sensitivity for the 60 GeV (40 GeV) measurement only, while the red curve is the combined result from both, obtained by summing the two signal yields; the "bump" at $m_{A'} \simeq 200$ MeV is due to the superposition of the accessible mass range in each measurement. The same results are reported in Fig. 27 as a function of y, considering again the case of a dark photon invisibly decaying to fermionic LDM, for the two values $\alpha_D = 0.1$ (left) and $\alpha_D = 0.5$ (right). In each plot, the black lines correspond to the aforementioned "targets" predicted by cosmology, in the hypothesis of a thermal LDM origin. To assess the variation of our result as a function of the LDM model fine details, we repeated the upper limit calculation considering also a scalar LDM model, finding very similar results. We also added in the same Figure the result (purple line) from a back-of-the-envelope sensitivity estimate for a 150 GeV run, considering a 75 GeV missing energy threshold and a 50% signal efficiency, in case of 10^{11} e^+OT and zero background events. We underline that this projection just highlights the potential of a future high-energy positron run, whose sensitivity requires a full background evaluation, in particular considering the much larger beam hadronic contamination. We leave this study for a future update of this proposal.

The complementarity of the proposed measurement with the approved NA64 100 GeV electron-beam program is highlighted by the fact that, operating at lower beam energy with a lower missing-energy threshold, the sensitivity of the proposed experimental program extends up to the A' mass values already explored by NA64, exploiting the secondary positrons in the electron-induced EM shower. We emphasize that the use of a positron beam will permit to maximally exploit LDM production via resonant e^+e^- annihilation, thus allowing to reach the LDM thermal targets with an accumulated statistics lower by one order or magnitude to that required for the electron-beam program.

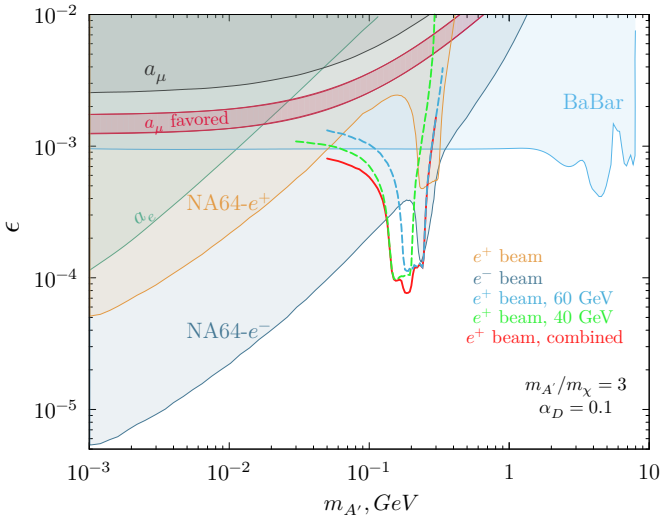

Figure 26. The projected sensitivity in the ε vs $m_{A'}$ space for the low-energy positron-beam measurements proposed in this work, for a total accumulated statistics of 10^{11} e^+OT, considering the benchmark scenario of fermionic LDM, with $\alpha_D = 0.1$. The most stringent LDM exclusion limits from BaBar [22] and NA64 [21] are also shown, as well as the favored area from the muon $g-2$ anomaly [26, 30] (red lines).

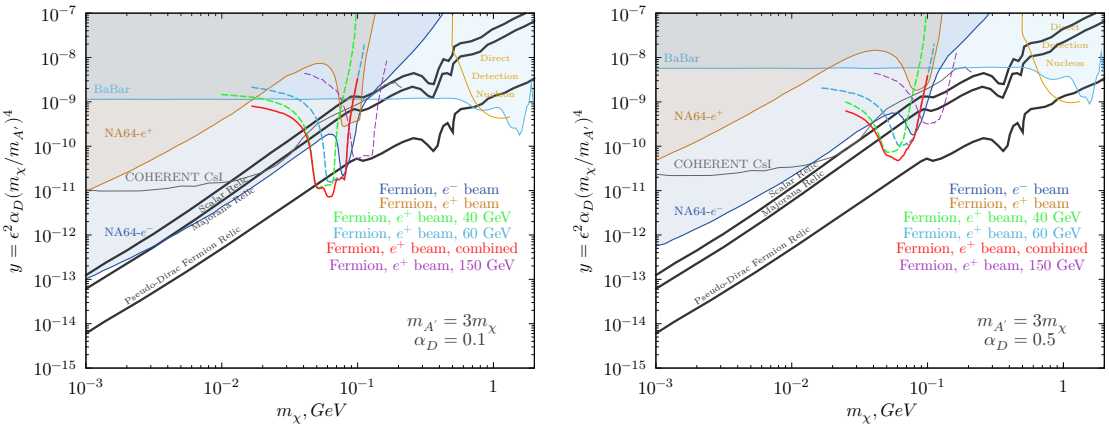

Figure 27. The projected sensitivity of the proposed positron measurements in the (y, m_χ) plane in the (m_χ, y) plane, for $\alpha_D = 0.1$ (left) and $\alpha_D = 0.5$ (right). The green and cyan curves are the results obtained from the detailed simulation of the 40 GeV and 60 GeV measurement, and the red curve correspond to their combination. The 150 GeV projection corresponds to a back-of-the-envelope calculation, assuming a zero-background condition. The other curves and shaded areas report already-existing limits in the same parameters space from NA64 in electron-beam mode [21], COHERENT [41], and BaBar [22]. The black lines show the favored parameter combinations for the observed dark matter relic density for different variations of the model.

6 Schedule, requests, and costs

6.1 Proposed experimental program

We propose to run the positron beam program after CERN LS3, performing multiple successive measurements during each year of operation, as summarized in Tab. 5. In preparation to this, a dedicated R&D phase during the 2024-2025 period.

6.1.1 The R&D program

The R&D phase is devoted to the experimental characterization of the new LYSO-based SRD detector technology, to the measurement of the intrinsic hadronic contamination of the H4 e^+ beam at 40 GeV and 60 GeV, and finally to the measurement of the main backgrounds expected during the experiment, in particular due to electro/photonuclear reactions occurring upstream the ECAL, to compare these with the Monte Carlo predictions and validate the latters.

- In 2024, we plan to dedicate one day of beam-time to measure the intrinsic hadronic contamination of the H4 positron beam at 40 GeV, 60 GeV and 150 GeV, following the methodology already adopted for the 100 GeV run presented in Ref. [27]. After this, we will dedicate two days of beam time to characterize the response of the LYSO SRD prototype, that will be installed in the NA64 setup at the location of the current SRD detector. We plan to measure the prototype response to a 100 GeV, a 60 GeV, and a 40 GeV e^+ beam, at different intensities up to $\sim 10^7$ e^+/spill, to assess the corresponding positron tagging efficiency and compare the results with Monte Carlo predictions. Finally, we plan to acquire data at 60 GeV for three days, to accumulate $\sim 3 \times 10^{10}$ e^+OT, and be able to characterize electro- and photo-nuclear induced backgrounds, by also varying the HCAL modules transverse position to measure the events lateral spread.

- In 2025, we plan to focus on the characterization of backgrounds at 40 GeV, by dedicating three days of beam time to accumulate up to $\sim 3 \times 10^{10}$ e^+OT with the

Year	Beam-time	Energy	e^+OT	Measurements goal
2024	1 week	40, 60, 150 GeV	-	Beam contamination studies, LYSO SRD *R&D*, backgrounds characterization at 60 GeV
2025	1 week	40 GeV	-	LYSO SRD *R&D*, backgrounds characterization at 40 GeV
2028	2 weeks	60 GeV	10^{11}	LDM thermal targets $\alpha_D = 0.1$, 175 MeV$\lesssim m_{A'} \lesssim$ 250 MeV
2029	2 weeks	40 GeV	10^{11}	LDM thermal targets $\alpha_D = 0.1$, 135 MeV$\lesssim m_{A'} \lesssim$ 180 MeV
2030	3 weeks	60 GeV	$\simeq 5 \times 10^{11}$	LDM thermal targets $\alpha_D = 0.5$, 135 MeV$\lesssim m_{A'} \lesssim$ 180 MeV
2031	3 weeks	40 GeV	$\simeq 5 \times 10^{11}$	
2032	2 weeks	150 GeV	10^{11}	LDM thermal targets $\alpha_D = 0.1$, 285 MeV$\lesssim m_{A'} \lesssim$ 390 MeV

Table 5. Summary of the beam-time requests for the positron beam program (for post-LS3 requests, we assumed 2028 to be the first year of operations). The 2024 and 2025 requests correspond to the pre-LS3 *R&D* program. The requests for 2028 and 2029 correspond, respectively, to the Phase-I and Phase-II measurements, for which a detailed reach estimate was presented in this document. Finally, requests for 2030, 2031 and 2032 are preliminary, and will be finalized in the future, based on the results from R&D and Phase-I/Phase-II measurements.

2023 detector configuration, followed by a similar measurement with the VHCAL installed just upstream the ECAL, as discussed in Sec. 4.

- R&D activity during LS3 (2026 - 2028). The results of the analysis of the data collected during 2024 and 2025 will be used to optimize the experimental setup in view of the proposed post-LS3 positron measurements. The priority will be given to the realization of the definitive SRD detector; the final design will be based on the data collected during 2024, allowing us to select the best crystal dimensions and arrangement, as well as the optimal light readout. Further setup R&D will be performed on the VHCAL and HCAL, including the increase of the longitudinal segmentation of the detectors, to improve the resolution and background rejection capability for the lower energy measurements. This work will be performed according to the results of the 2024-2025 measurements of the electro- and photo-nuclear induced background, together with monte carlo simulations.

6.1.2 The experimental program

In order to maximize the efficiency of the use of the H4 beamline, we propose to run the low-energy NA64 e^+ measurements directly at the end of the beam-time allocated for the NA64 100-GeV electron beam missing-energy measurement, staggering them in multiple years to minimize the impact on the main experimental program. This will allow to minimize the effort devoted to the setup installation, and to run only once the measurements dedicated to the detector commissioning and calibration, thus saving a significant amount of beam-time. We underline that, other than the new experimental apparatus discussed previously, no other modifications to the existing NA64 detector configuration or setup will be required to run this program. Similarly, no further requirements in terms of new services or infrastructures are expected, other than those already in use for the NA64 setup at H4.

- The Phase-I measurement will be performed in the first year after CERN LS3, running with a 60 GeV positron beam. We will acquire data with average beam intensity equal to $\simeq 5 \times 10^6$ e^+OT/spill, thus allowing to accumulate up to 10^{11} positrons-on-target within 7 days of run, assuming 3500 spills/day. During Phase-I, the new SRD detector will be used. Considering that the new high-performance SRD detector will be used also during the main NA64-e program, we expect to install it and commission it already during the preceding 100 GeV electron-beam run. Therefore, no dedicated beam-time is required for this task.

- During Phase-II, planned in the second year after CERN LS3, a 40 GeV positron beam measurement will be performed accumulating up to 10^{11} e^+OT, operating with the same Phase-I beam intensity. In the measurement, we'll possibly replace the current NA64 active target with the new $PbWO_4$ calorimeter. Since this will be the first time that this new detector will be used in NA64, we foresee three days of beam-time dedicated to commissioning and calibration, followed again by 10 days of

Item	Price
$PbWO_4$ calorimeter	500 kCHF
SRD detector	200 kCHF
Total	$\sim$ 700 kCHF

Table 6. Cost estimate for the new SRD and $PbWO_4$ detectors employed in the proposed positron-beam measurements.

run to reach the required statics. Overall, approximately two weeks of beam-time will be requested for Phase-II.

After Phase-II, we propose to extend the positron-beam program with further measurements, eventually also at different beam energy, to explore new regions of the parameter space, probing the thermal targets for higher masses and for different values of the α_D parameter. A detailed plan for Phase-III and following runs will be defined in the future, based on the results from the *R&D* and Phase-I/Phase-II measurements. At this moment, we envisage to accumulate further statistics at 40 GeV and 60 GeV, significantly increasing the beam intensity to up to $(2-3)\times 10^7$ e^+OT/spill to probe the LDM thermal targets in the mass range 135 MeV $\lesssim m_{A'} \lesssim$ 250 MeV also for $\alpha_D = 0.5$. Subsequently, we foresee to possibly execute one run at even higher beam energy (150 GeV), to explore the $m_{A'}$ values in the range 270 MeV$\lesssim m_{A'} \lesssim$ 390 MeV. The sensitivity of this measurement has to be properly defined from a thoughtful study of the backgrounds due to beam hadronic contamination, predicted to be of about 70%, one order of magnitude higher than the 100 GeV value. Furthermore, we also expect to re-discuss the opportunity for the 150 GeV at the beginning of the post-LS3 program, also in light of first results and future plans for the NA64$-\mu$ program [42], particularly sensitive to the large A' mass region.

6.2 Costs

A preliminary estimate of the expected costs is presented in Tab. 6. We stress that all costs associated with the $PbWO_4$ calorimeter construction are covered by the POKER ("Positron resonant annihilation intO darK mattER") ERC project[11], whose scientific goal is to demonstrate the feasibility of a positron-beam, missing-energy measurement to search for Light Dark Matter resonantly produced by electron-positron annihilation. Part of the costs for the new SRD construction are supported by the synergistic SOCIO project[12], aiming to tackle a dedicated technological R&D program to identify for each component involved in the positron-beam missing energy experiment the main challenges associated to the transition from a small-scale demonstration to a full-scale experiment.

[11]The POKER ERC project has received funding from the European Research Council (ERC) under the European Union's Horizon 2020 research and innovation programme, Grant agreement No. 947715.
[12]The SOCIO is funded by the Italian Ministry for Research under the FARE-2020 program.

7 Conclusions

The availability of a high-energy and high-intensity positron beam at CERN SPS provides a unique opportunity for Dark Sector studies aiming to search for Light Dark Matter, exploiting the dark photon production channel via resonant e^+e^- annihilation and its subsequent decay to LDM. The possibility to easily reconfigure the beam energy will allow to start a dedicated, multi-phase program, made by multiple measurements to "scan" the mass range in the 140 MeV$\lesssim m_{A'} \lesssim$ 250 MeV interval. The proposed measurement will probe this LDM parameters space down to the "thermal target", confirming or ruling out the light dark matter hypothesis. The positron program is fully complementary to those obtained from the main NA64 experimental program with a 100 GeV positron beam, where secondary positrons in the developing EM shower allow to explore the mass range 140 MeV$\lesssim m_{A'} \lesssim$ 250 MeV through the same production channel.

We propose to perform a multi-phase experimental program, preceded by a dedicated R&D phase, mainly devoted to backgrounds characterization and detector optimization, to be carried out before LS3.

At the beginning, we plan to execute a first 60 GeV beam energy measurement, followed by a second one at 40 GeV. Both measurements will be performed at the H4 beamline, exploiting the current NA64 detector setup. Two detector elements - the SRD and the active target - will be upgraded to match the new requirements introduced by the lower-energy kinematic regime. Furthermore, we will improve the overall detector setup, for example by optimizing the position of the VHCAL detector, or using for the first HCAL module the one with larger transverse dimensions already developed for the NA64$-\mu$ program.

For both measurements, we anticipate to collect 10^{11} e^+OT within few weeks of run. To optimize the use of the H4 beamline, we plan to carry out each measurement at the end of the electron-beam run, thus minimizing the time devoted to detector commissioning and calibration. A detailed study of the expected background yield, based on a combination of Monte Carlo simulations and data-driven estimates, showed that, for this configuration, both positron-beam measurements are expected to be background-free. Thanks to this, the expected sensitivity will allow these measurements to probe the LDM parameters space down to the "thermal target", definitively confirming or ruling out the light dark matter hypothesis in the mass range 135 MeV$\lesssim m_{A'} \lesssim$ 250 MeV, for $\alpha_D = 0.1$.

Based on the obtained results, we envisage to extend this program with future runs performed at higher beam energy (150 GeV), in order to explore the mass range 285 MeV$\lesssim m_{A'} \lesssim$ 390 MeV, and at higher intensity, up to $(2-3)\times10^7$ e^+OT/spill, to probe the thermal targets in the mass region a135 MeV $\lesssim m_{A'} \lesssim$ 250 MeV also for $\alpha_D = 0.5$.

Finally, we remark that, although the resonant e^+e^- annihilation approach is primary focused on the probing of the LDM model with the A' mediator, the proposed accurate measurements of the missing-energy rate with e^+ beams at different energies provide also a sensitive test of Dark Sector physics with a variety of other light mediator particles, such e.g. scalar, pseudoscalar, $L_\mu - L_\tau$ and $B - L$ Z' bosons [43, 44].

A Resonant LDM production by positrons annihilation on atomic electrons

The resonant cross section for a vector A' decaying to fermionic or scalar LDM reads:

$$\sigma_{res} = \frac{4\pi\alpha_{EM}\alpha_D\varepsilon^2}{\sqrt{s}} \frac{q\mathcal{K}}{(s - m_{A'}^2)^2 + \Gamma_{A'}^2 m_{A'}^2 \eta} \ , \tag{A.1}$$

where s is the e^+ e^- system invariant mass squared, q is the LDM daughter particles momentum in the CM frame, and $\Gamma_{A'}$ is the A' width, given by

$$\begin{aligned} \Gamma_{A'} &= \alpha_D \frac{m_{A'}}{3}(1 + 2r^2)\sqrt{1 - 4r^2}\,\text{(fermionic LDM)} \\ \Gamma_{A'} &= \alpha_D \frac{m_{A'}}{12}(1 - 4r^2)^{3/2} \ \text{(scalar LDM)}, \end{aligned} \tag{A.2}$$

where $r \equiv m_\chi/m_{A'}$, and we neglected the ε^2-suppressed A' visible decay channel. Finally, $\mathcal{K}$ is a kinematic factor equal to $s - 4/3q^2$ $(2/3q^2)$ for the fermionic (scalar) case, while $\eta = (s/m_{A'}^2)^2$ is a correction term introduced for the fermionic LDM case ($\alpha_D = 0.5$) to consider the energy dependence of $\Gamma_{A'}$ when this is non-negligible with respect to $m_{A'}$.

This cross section exhibits a maximum at $s = m_{A'}^2$, i.e. at positron energy $E_R \simeq m_{A'}^2/(2m_e)$. By energy conservation, $E_{e^+} \simeq E_{A'} = E_\chi + E_{\overline{\chi}}$: the distribution of the energy sum of the final state LDM pair and, by extension, of the $s-$channel dark photon also shows a maximum at this energy value.

The expected differential energy distribution of the dark photons produced in the thick target scales as $n(E_{A'}) \propto \sigma_{res}(E_{e^+})T(E_{e^+})$, where T is the secondary positrons' track-length distribution [17, 45, 46]. While for low mass values the resonant peak at $E_{A'} = E_R$ is clearly visible, for higher $m_{A'}$ values, corresponding to the case $E_R > E_0$, the dominant contribution to the signal yield, also due to the shape of $T(E_{e^+})$, is associated with the decays of off-shell A' produced at the low-energy tail of σ_{res} and thus the peak is no longer present. The expected number of signal events with A' energy greater than a threshold E_{miss}^{thr} is given by:

$$N_{Sig} = N_{EOT}\frac{N_A}{A} Z\rho \int_{E_{miss}^{thr}}^{E_0} dE_{e^+}\ T(E_{e^+})\,\widetilde{\sigma}_{res}(E_{e^+}) \tag{A.3}$$

where A, Z, ρ, are, respectively, the thick target atomic mass, atomic number, and mass density, N_A is Avogadro's number, and N_{EOT} is the number of impinging electrons. Finally, $\widetilde{\sigma}_{res}$ is the annihilation cross section convoluted with the active thick target energy resolution.

B Additional documentation for the new SRD

B.1 Afterpulse

The high hit rate of the SRD in NA64 (≈1 MHz) may lead to critical pile-up effects, undermining the capability to reject beam contaminants. To verify this effect, a dedicated R&D aimed at testing an 8×8 matrix of LYSO/LSO crystals of 3×3×25 mm^3 each (see Fig. 28) has been performed at the SPS beam line H8, during the 30^{th} week of testing in the North Area in Summer 2022.

Figure 28. A 8×8 matrix of LYSO/LSO crystals. To maximize light-gathering, the crystal matrix is coated with reflective foils.

For this test, the crystals were coupled to a SiPM MPPC array S13361-3050AE-08 by Hamamatsu. The SiPMs HV supply and readout were carried out through a dedicated PCB, and the signal amplification entrusted to a custom amplifier. The test was conducted by reading the signals of a single crystal. The matrix was placed in a 3D-printed dark box, which was positioned along the beam line such that it impinged on the crystals' faces. Together with the array, two plastic scintillators were placed along the beam line, and data taking was conducted requiring a triple coincidence between these detectors. To verify the presence of any afterpulse events, a large acquisition time window of 10 microseconds was chosen. For this measurement, a muon beam of energy 160 GeV was used. The waveforms of a typical event are shown in Fig. 29.

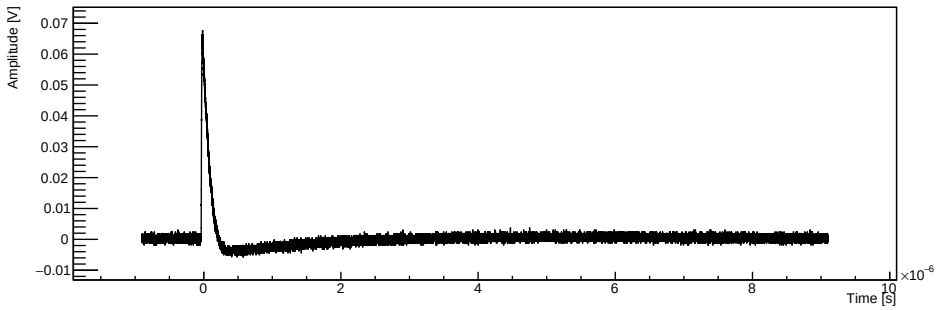

Figure 29. Typical waveform of a muon event in the LYSO matrix.

The waveform illustrated in the figure shows the peak due to the muon event, as well as the subsequent region (10 microseconds long) in which the afterpulse events are searched.

The peak has a width equal to ≈150 ns (which is far greater than the typical LYSO decay time, up to tens of nanoseconds), and presents an "overshoot" at its very end: both these effects are attributable to the signal reading electronics, which had not been optimized for this purpose. Over the entire duration of the measurement, a statistics of 7743 muon events were collected. During the data analysis phase, an algorithm was developed to search for afterpulse events: firstly, a template fit was constructed by choosing 10 random events that did not present afterpulse. These files were sampled and averaged to obtain the $g(t)$ function. The fit function $f(t)$ is defined as:

$$f(t) = p_0 \cdot g(p_1(t - p_2)) \tag{B.1}$$

Where p_0, p_1, and p_2 are three parameters that take into account, respectively, any vertical shifts, enlargements, and horizontal shifts of the peak. All waveforms were fitted in the peak region, and, finally, to search for afterpulse events, the presence of at least two consecutive amplitude values that exceeded the corresponding value of the function $f(t)$ by at least 3σ was required (σ being the standard deviation of the amplitude, calculated in a waveform region before the peak). This procedure led to the identification of 13 afterpulse events (0.17% of the total recorded events). Therefore, from this first test, it is possible to conclude that the fraction of afterpulse events is not high enough to potentially affect our measurements. Indeed, further studies (with greater statistics) will be performed to confirm this result.

B.2 Intrinsic radioactivity

Another important aspect to consider for the evaluation of LYSO/LSO for our purposes is its intrinsic radioactivity, due to the presence of ^{176}Lu, which decays by emitting beta and gamma particles [47]. As discussed above, this may lead to background events if a decay (or a double decay) happens in coincidence with the passage of a hadron contaminant. To understand the extent of this phenomenon, we carried out Monte Carlo simulations of the decays of ^{176}Lu in a 14×5 LYSO/LSO crystal matrix. The distribution of energy deposited in the crystals was then studied and the fraction of background events that survived the cuts was estimated. The cuts were optimized based on the simulations of the synchrotron energy deposition in the matrix, with 40 and 60 GeV positron beams. In light of these simulations, a threshold on the energy deposited in the individual crystals equal to 100 phe (corresponding to 330 keV[13].) was chosen. We then looked at the distribution of the number of crystals with an energy deposition greater than the threshold, both for the signal events (simulations at 40 and 60 GeV) and for the background events, i.e. intrinsic radioactivity. The results are shown in Fig. 30

[13]The conversion from photoelectrons to energy is performed following the outcomes of a characterization of a LYSO/LSO crystal of dimensions 1.5×1.5×16 cm^3 carried out with a ^{60}Co source.

Multiplicity	η_{40GeV}	η_{60GeV}	η_{1d}	η_{2d}
1	0.973	0.999	0.929	0.995
2	0.888	0.999	0.01	0.855
3	0.747	0.997	0	0.018

Table 7. Fraction of signal and background events that survive the energy cutoff of 100 phe at different multiplicity cutoffs, where η_{1d} (η_{2d}) is the fraction of single (double) decay events surviving the cuts.

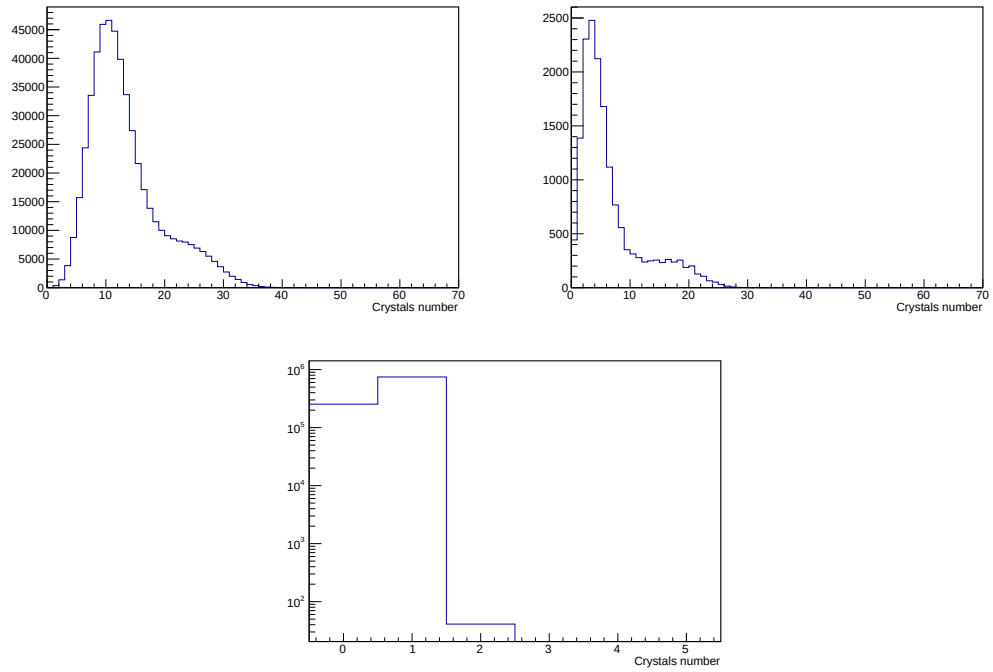

Figure 30. Distribution of the number of crystals bearing deposited energy above the 100 phe threshold for the 60 (40) GeV e^+ beam simulation on the left (right). Below, the same distribution for the ^{176}Lu decays simulation is reported.

As shown in the figure, at 60 (40) GeV each event typically deposits enough energy to cause 10 (4) crystals to exceed the threshold of 100 photoelectrons. In simulations of the intrinsic radioactivity, however, typically each event that exceeds the energy threshold lights up at most 2 crystals. It was therefore possible to set, in addition to an energy threshold, a "multiplicity" threshold, i.e. a condition that requires a deposition of energy greater than 100 phe in at least 2 or 3 crystals. By applying both an energy and multiplicity cut, we obtain the efficiencies (expressed as the fraction of events that survive the cuts) illustrated in Tab. 7. Where η_{40GeV} (η_{60GeV}) is the fraction of synchrotron photon events generated by a 40 (60) GeV e^+ surviving the cuts, while η_{1d} (η_{2d}) is the fraction of single (double) decay events surviving the cuts. To maximize the fraction of synchrotron radiation events produced by positrons of energy 40 GeV, it was decided to set a multiplicity threshold equal to 2. Once the fraction of background events is known, it is possible to calculate the

single (P_{1d}) or double (P_{2d}) decay probability in a time window equal to 50 ns, according to:

$$\begin{aligned} P_{1d} &= A \cdot \Delta t \cdot \eta_{1d} \\ P_{2d} &= 2 \cdot A^2 \cdot \Delta t^2 \cdot \eta_{2d} \end{aligned} \tag{B.2}$$

Where A is the activity of the whole LYSO/LSO matrix and Δt is the coincidence time of 50 ns. Last, starting from the extent of hadronic contamination ($\frac{h}{e}$) at 40 and 60 GeV, it is possible to calculate the hadronic background rate (R_h) according to:

$$\mathrm{R}_h = \mathrm{R}_{e^+} \cdot \frac{h}{e} \cdot (P_{1d} + P_{2d}) \tag{B.3}$$

This procedure was carried out on simulations of a 14×5 matrix and a 14×3 matrix, leading to the results in Tab. 2, for which a multiplicity cut equal to 2 was chosen.

References

[1] Y. M. Andreev et al. (2023).

[2] G. Bertone and D. Hooper. *Rev. Mod. Phys.* 90, 045002 (2018). doi:10.1103/RevModPhys.90.045002.

[3] A. R. Liddle. *An introduction to modern cosmology* (1998).

[4] G. Arcadi, et al. *Eur. Phys. J. C* 78, 203 (2018). doi:10.1140/epjc/s10052-018-5662-y.

[5] B. Holdom. *Phys. Lett. B* 166, 196 (1986). doi:10.1016/0370-2693(86)91377-8.

[6] S. Knapen, T. Lin, and K. M. Zurek. *Phys. Rev. D* 96, 115021 (2017). doi:10.1103/PhysRevD.96.115021.

[7] R. Essig, et al. On the Origin of Light Dark Matter Species (2010).

[8] F. del Aguila, G. D. Coughlan, and M. Quiros. *Nucl. Phys. B* 307, 633 (1988). doi:10.1016/0550-3213(88)90266-0. [Erratum: Nucl. Phys. B **312**, 751(E) (1989)].

[9] N. Arkani-Hamed and N. Weiner. *JHEP* 12, 104 (2008). doi:10.1088/1126-6708/2008/12/104.

[10] M. Battaglieri et al. In *U.S. Cosmic Visions: New Ideas in Dark Matter* (2017).

[11] M. Fabbrichesi, E. Gabrielli, and G. Lanfranchi (2020). doi:10.1007/978-3-030-62519-1. SpringerBrief in Physics.

[12] A. Filippi and M. De Napoli. *Rev. Phys.* 5, 100042 (2020). doi:10.1016/j.revip.2020.100042.

[13] J. Beacham et al. *J. Phys. G* 47, 010501 (2020). doi:10.1088/1361-6471/ab4cd2.

[14] P. Ilten et al. In *Snowmass 2021* (2022).

[15] M. Graham, C. Hearty, and M. Williams (2021).

[16] S. N. Gninenko, et al. *Phys. Rev. D* 94, 095025 (2016). doi:10.1103/PhysRevD.94.095025.

[17] L. Marsicano, et al. *Phys. Rev. Lett.* 121, 041802 (2018). doi:10.1103/PhysRevLett.121.041802.

[18] L. Marsicano, et al. *Phys. Rev. D* 98, 015031 (2018). doi:10.1103/PhysRevD.98.015031.

[19] E. Izaguirre, et al. *Phys. Rev. D* 88, 114015 (2013). doi:10.1103/PhysRevD.88.114015.

[20] Y. M. Andreev et al. *Phys. Rev. D* 104, L091701 (2021). doi:10.1103/PhysRevD.104.L091701.

[21] Y. M. Andreev et al. *Phys. Rev. Lett.* 131, 161801 (2023). doi:10.1103/PhysRevLett.131.161801.

[22] J. P. Lees et al. *Phys. Rev. Lett.* 119, 131804 (2017). doi:10.1103/PhysRevLett.119.131804.

[23] R. Essig, et al. *JHEP* 11, 167 (2013). doi:10.1007/JHEP11(2013)167.

[24] E. Cortina Gil et al. *JHEP* 05, 182 (2019). doi:10.1007/JHEP05(2019)182.

[25] P. Fayet. *Phys. Rev. D* 75, 115017 (2007). doi:10.1103/PhysRevD.75.115017.

[26] B. Abi et al. *Phys. Rev. Lett.* 126, 141801 (2021). doi:10.1103/PhysRevLett.126.141801.

[27] Y. M. Andreev et al. *Nucl. Instrum. Meth. A* 1057, 168776 (2023). doi:10.1016/j.nima.2023.168776.

[28] M. Bondi, et al. *Comput. Phys. Commun.* 269, 108129 (2021). doi:10.1016/j.cpc.2021.108129.

[29] D. Banerjee et al. *Phys. Rev. D* 97, 072002 (2018). doi:10.1103/PhysRevD.97.072002.

[30] M. Pospelov. *Phys. Rev. D* 80, 095002 (2009). doi:10.1103/PhysRevD.80.095002.

[31] G. Brianti. SPS North Experimental Area. Technical report, CERN, Geneva (1973).

[32] A. C. Booth, et al. *Phys. Rev. Accel. Beams* 22, 061003 (2019). doi:10.1103/PhysRevAccelBeams.22.061003.

[33] S. N. Gninenko, N. V. Krasnikov, and V. A. Matveev. *Physics of Particles and Nuclei* 51, 829 (2020). doi:10.1134/s1063779620050044.

[34] P. Bisio, et al. Measurement of the intrinsic hadronic contamination in the NA64$-e$ high-purity e^+/e^- beam at cern (2023).

[35] C. Wanarak, W. Chewpraditkul, and A. Phunpueok. *Procedia Engineering* 32, 765 (2012). doi:https://doi.org/10.1016/j.proeng.2012.02.010. ISEEC.

[36] S. Seifert, et al. *Journal of Instrumentation* 7, P09004 (2012). doi:10.1088/1748-0221/7/09/P09004.

[37] R. L. Workman et al. *PTEP* 2022, 083C01 (2022). doi:10.1093/ptep/ptac097.

[38] C. Biino. *J. Phys. Conf. Ser.* 587, 012001 (2015). doi:10.1088/1742-6596/587/1/012001.

[39] R. R. Dusaev, D. V. Kirpichnikov, and M. M. Kirsanov. *Phys. Rev. D* 102, 055018 (2020). doi:10.1103/PhysRevD.102.055018.

[40] D. Banerjee et al. *Phys. Rev. Lett.* 125, 081801 (2020). doi:10.1103/PhysRevLett.125.081801.

[41] D. Akimov et al. *Phys. Rev. Lett.* 130, 051803 (2023). doi:10.1103/PhysRevLett.130.051803.

[42] H. Sieber, et al. *Phys. Rev. D* 105, 052006 (2022). doi:10.1103/PhysRevD.105.052006.

[43] Y. M. Andreev et al. *Phys. Rev. Lett.* 129, 161801 (2022). doi:10.1103/PhysRevLett.129.161801.

[44] Y. M. Andreev et al. *Phys. Rev. D* 106, 032015 (2022). doi:10.1103/PhysRevD.106.032015.

[45] A. Chilton. *Health Physics* 34, 715 (1978).

[46] Y.-S. Tsai and V. Whitis. *Phys. Rev.* 149, 1248 (1966). doi:10.1103/PhysRev.149.1248.

[47] M. Hult, et al. *Applied Radiation and Isotopes* 87, 112 (2014). doi:https://doi.org/10.1016/j.apradiso.2013.11.071. Proceedings of the 19th International Conference on Radionuclide Metrology and its Applications 17-21 June 2013, Antwerp, Belgium.